$K^*(892)^0$ and $\phi(1020)$ meson production at high transverse momentum in pp and Pb-Pb collisions at $\sqrt{s_{NN}} = 2.76$ TeV

J. Adam *et al.*[*]
(ALICE Collaboration)

(Received 17 February 2017; published 12 June 2017)

The production of $K^*(892)^0$ and $\phi(1020)$ mesons in proton-proton (pp) and lead-lead (Pb-Pb) collisions at $\sqrt{s_{NN}} = 2.76$ TeV has been analyzed using a high luminosity data sample accumulated in 2011 with the ALICE detector at the Large Hadron Collider (LHC). Transverse momentum (p_T) spectra have been measured for $K^*(892)^0$ and $\phi(1020)$ mesons via their hadronic decay channels for p_T up to 20 GeV/c. The measurements in pp collisions have been compared to model calculations and used to determine the nuclear modification factor and particle ratios. The $K^*(892)^0/K$ ratio exhibits significant reduction from pp to central Pb-Pb collisions, consistent with the suppression of the $K^*(892)^0$ yield at low p_T due to rescattering of its decay products in the hadronic phase. In central Pb-Pb collisions the p_T dependent $\phi(1020)/\pi$ and $K^*(892)^0/\pi$ ratios show an enhancement over pp collisions for $p_T \approx 3$ GeV/c, consistent with previous observations of strong radial flow. At high p_T, particle ratios in Pb-Pb collisions are similar to those measured in pp collisions. In central Pb-Pb collisions, the production of $K^*(892)^0$ and $\phi(1020)$ mesons is suppressed for $p_T > 8$ GeV/c. This suppression is similar to that of charged pions, kaons, and protons, indicating that the suppression does not depend on particle mass or flavor in the light quark sector.

DOI: 10.1103/PhysRevC.95.064606

I. INTRODUCTION

It has been established that hot and dense strongly interacting matter, often described as a strongly coupled quark-gluon plasma (sQGP) [1–3], is produced in heavy-ion collisions at ultrarelativistic energies. The properties of this matter are characterized, among other features, by the energy loss of partons traversing the dense color-charged medium, which manifests itself via suppression of hadrons with high transverse momentum in central Pb-Pb collisions. The hadrons that contain light (up, down, and strange) valence quarks exhibit a suppression similar to that of particles containing heavy quarks (charm) both at the Relativistic Heavy Ion Collider (RHIC) [4,5] and at the Large Hadron Collider (LHC) [6,7]. The apparent particle species independence of high-p_T hadron suppression is a challenge for models [8–10]. Since $K^*(892)^0$ ($d\bar{s}$), $\overline{K}^*(892)^0$ ($\bar{d}s$), and $\phi(1020)$ ($s\bar{s}$) contain strange (or antistrange) quarks, they are used here for a systematic study of the particle species dependence of the partonic energy loss in the medium. Moreover, the measurements of high-p_T differential yields can be used to test perturbative QCD inspired model calculations.

The system produced in heavy-ion collisions evolves through different stages, with a transition from partonic to hadronic matter around a temperature $T_c \approx 156$ MeV [11–13]. The $K^*(892)^0$ and $\phi(1020)$ life times in vacuum are 4.16 ± 0.05 fm/c and 46.3 ± 0.4 fm/c, respectively [14]. Due to their short lifetimes, resonances can be used to probe the system at different timescales during its evolution and have been proven to be very useful in exploring various aspects of heavy-ion collisions [15]. Yields of resonances measured via hadronic decay channels can be affected by particle rescattering and regeneration in the hadron gas phase. The momentum dependence of rescattering and regeneration may also modify the observed momentum distributions of the reconstructed resonances.

Resonances like $K^*(892)^0$ and $\phi(1020)$ can also contribute to a systematic study of the enhancement of baryon-to-meson ratios (e.g., p/π and Λ/K^0_S [16,17]) at intermediate p_T. Recombination models suggest that the number of constituent quarks of the hadrons determine the enhancement, while hydrodynamic models explain this on the basis of differences in the hadron masses leading to different radial flow patterns. The $K^*(892)^0$ and $\phi(1020)$ mesons, which have masses very close to that of a proton, are well suited for testing the underlying hadron production mechanisms.

In this paper, $K^*(892)^0$ and $\phi(1020)$ meson production in pp and Pb-Pb collisions at $\sqrt{s_{NN}} = 2.76$ TeV is studied. We have previously published measurements of $K^*(892)^0$ and $\phi(1020)$ meson production for $p_T < 5$ GeV/c in Pb-Pb collisions at $\sqrt{s_{NN}} = 2.76$ TeV [18] using data recorded in 2010. The high luminosity data taken by ALICE in 2011 allow statistically improved signal measurements. The spectra have been measured in the range $0 < p_T < 15$ GeV/c ($0.4 < p_T < 21$ GeV/c) in minimum bias pp collisions and $0.3 < p_T < 20$ GeV/c ($0.5 < p_T < 21$ GeV/c) in Pb-Pb collisions in six [seven] centrality classes for $K^*(892)^0$ [$\phi(1020)$]. This new data set also allowed the measurement of $K^*(892)^0$ in finer centrality intervals in central and semicentral Pb-Pb collisions to study hadron production mechanisms at low, intermediate, and high p_T. The new measurements of $K^*(892)^0$ and $\phi(1020)$ meson production in pp collisions at $\sqrt{s} = 2.76$ TeV are used

[*]Full author list given at the end of the article.

to calculate particle ratios and also to test various perturbative QCD inspired event generators.

The nuclear modification factor (R_{AA}) is defined as the yield of particles in heavy-ion collisions relative to that in elementary pp collisions, scaled with the average nuclear overlap function.

$$R_{AA} = \frac{1}{\langle T_{AA}\rangle} \times \frac{(d^2N/dy\,dp_T)_{AA}}{(d^2\sigma/dy\,dp_T)_{pp}}, \quad (1)$$

where $\langle T_{AA}\rangle = \langle N_{\rm coll}\rangle/\sigma_{\rm inel}$ is the average nuclear overlap function, $\langle N_{\rm coll}\rangle$ is the average number of binary nucleon-nucleon collisions calculated using Monte Carlo (MC) Glauber [19] simulations, and $\sigma_{\rm inel}$ is the inelastic pp cross section [20].

Throughout this paper, the results for $K^*(892)^0$ and $\overline{K}^*(892)^0$ are averaged and denoted by the symbol K^{*0}, and $\phi(1020)$ is denoted by ϕ unless specified otherwise. The paper is organized as follows: Section II describes the data analysis techniques. Section III presents results including K^{*0} and ϕ meson $p_{\rm T}$ spectra, ratios to different hadrons, and nuclear modification factors. A summary is given in Sec. IV.

II. DATA ANALYSIS

New measurements of K^{*0} and ϕ meson production have been performed on data taken with the ALICE detector in the year 2011. The resonances are reconstructed via hadronic decay channels with large branching ratios (BR): $K^{*0} \to \pi^{\pm}\mathrm{K}^{\mp}$ with BR 66.6% and $\phi \to \mathrm{K}^+\mathrm{K}^-$ with BR 48.9% [14]. For both K^{*0} and ϕ, the measurements are performed in six common centrality classes: 0–5%, 5–10%, 10–20%, 20–30%, 30–40%, 40–50%. The peripheral centrality class 60–80% is also measured for ϕ only.

A. Event and track selection

The data in pp collisions were collected in 2011 using a minimum bias (MB) trigger, requiring at least one hit in any of the V0-A, V0-C, and Silicon Pixel Detectors (SPDs), in coincidence with the presence of an LHC bunch crossing [21,22]. The ALICE V0 are small-angle plastic scintillator detectors placed on either side of the collision vertex, covering the pseudorapidity ranges $2.8 < \eta < 5.1$ (V0-A) and $-3.7 < \eta < -1.7$ (V0-C). The two SPD layers, which cover $|\eta| < 2.0$, are the innermost part of the the Inner Tracking System (ITS), composed of six layers of silicon detector placed radially between 3.9 and 43 cm around the beam pipe. During the high luminosity Pb-Pb run in 2011, V0 online triggers were used to enhance central 0–10%, semicentral 10–50%, and select MB (0–80%) events. The trigger was 100% efficient for the 0–8% most central Pb-Pb collisions and 80% efficient for centrality 8–10% [23]. The inefficiency for the 8–10% range has a negligible (<1%) effect on the results presented in this paper. The numbers of events after event selections are summarized in Table I.

A detailed description of the ALICE detector is given in Refs. [24–26]. The ALICE Inner Tracking System (ITS) and the Time Projection Chamber (TPC), are used for tracking and reconstruction of the primary vertex. Events are required to have the primary vertex coordinate along the beam axis (v_z) within 10 cm from the nominal interaction point. Tracks in the TPC are selected for both K^{*0} and ϕ reconstruction with the requirement of at least 70 TPC pad rows measured along the track out of a maximum possible 159. The TPC covers the pseudorapidity range $|\eta| < 0.9$ with full azimuthal acceptance. To ensure a uniform acceptance, the tracks are selected within $|\eta| < 0.8$. The data sample for the pp analysis is chosen to have minimal pileup; Pb-Pb collisions have negligible pileup. In order to reduce contamination from beam-background events and secondary particles coming from weak decays, cuts on the distance of closest approach to the primary vertex in the xy plane (DCA_{xy}) and z direction (DCA_z) are applied. The value of DCA_{xy} is required to be less than 7 times its resolution, $\mathrm{DCA}_{xy}(p_{\rm T}) < 0.0105 + 0.035\,p_{\rm T}^{-1.1}$ cm ($p_{\rm T}$ in GeV/c), and DCA_z is required to be less than 2 cm. The $p_{\rm T}$ of each track is restricted to be greater than 0.15 GeV/c for K^{*0} in pp and Pb-Pb collisions and for ϕ in pp collisions. For ϕ in Pb-Pb collisions the track $p_{\rm T}$ was required to be >0.75 GeV/c for the 0–5% centrality class and >0.5 GeV/c otherwise. The higher $p_{\rm T}$ cut for the ϕ analysis without particle identification (PID) was needed to improve the signal-to-background ratio at low momentum.

TABLE I. Summary of different trigger selected data sets and number of events analyzed in pp and Pb-Pb collisions at $\sqrt{s_{NN}} =$ 2.76 TeV.

Centrality	Events	Year	Data set
0–10%	2.0×10^7	2011	Pb-Pb
10–50%	1.8×10^7	2011	Pb-Pb
0–80%	6.0×10^5	2011	Pb-Pb
MB	3.0×10^7	2011	pp

The TPC has been used to identify charged particles by measuring the specific ionization energy loss (dE/dx). For K^{*0} reconstruction, both in pp and Pb-Pb collisions, pion and kaon candidates are required to have mean values of the specific energy loss in the TPC ($\langle dE/dx\rangle$) within two standard deviations ($2\sigma_{\rm TPC}$) of the expected dE/dx values for each particle species over all momenta. In the case of ϕ meson reconstruction, two PID selection criteria depending on the $p_{\rm T}$ of the ϕ meson are used. In both pp and Pb-Pb collisions the narrow ϕ signal is extracted from the unidentified two-particle invariant-mass distribution for $p_{\rm T} > 1$ GeV/c. In pp collisions the production of the ϕ meson is additionally measured with a $2\sigma_{\rm TPC}$ restriction on $\langle dE/dx\rangle$ for $0.4 < p_{\rm T} < 5$ GeV/c. The spectra measured without PID in Pb-Pb collisions are comparable with the published 2010 results [18] obtained with PID. Measurements with and without PID are found to be in good agreement for both collision systems in the overlap region ($1 < p_{\rm T} < 5$ GeV/c). The $p_{\rm T}$ spectra in this paper are combinations of results obtained with PID at low momentum ($p_{\rm T} < 3$ GeV/c) and results obtained without PID for higher $p_{\rm T}$ in both pp and Pb-Pb collisions.

B. Yield extraction

The K^{*0} (ϕ) is reconstructed through its dominant hadronic decay channel by calculating the invariant-mass

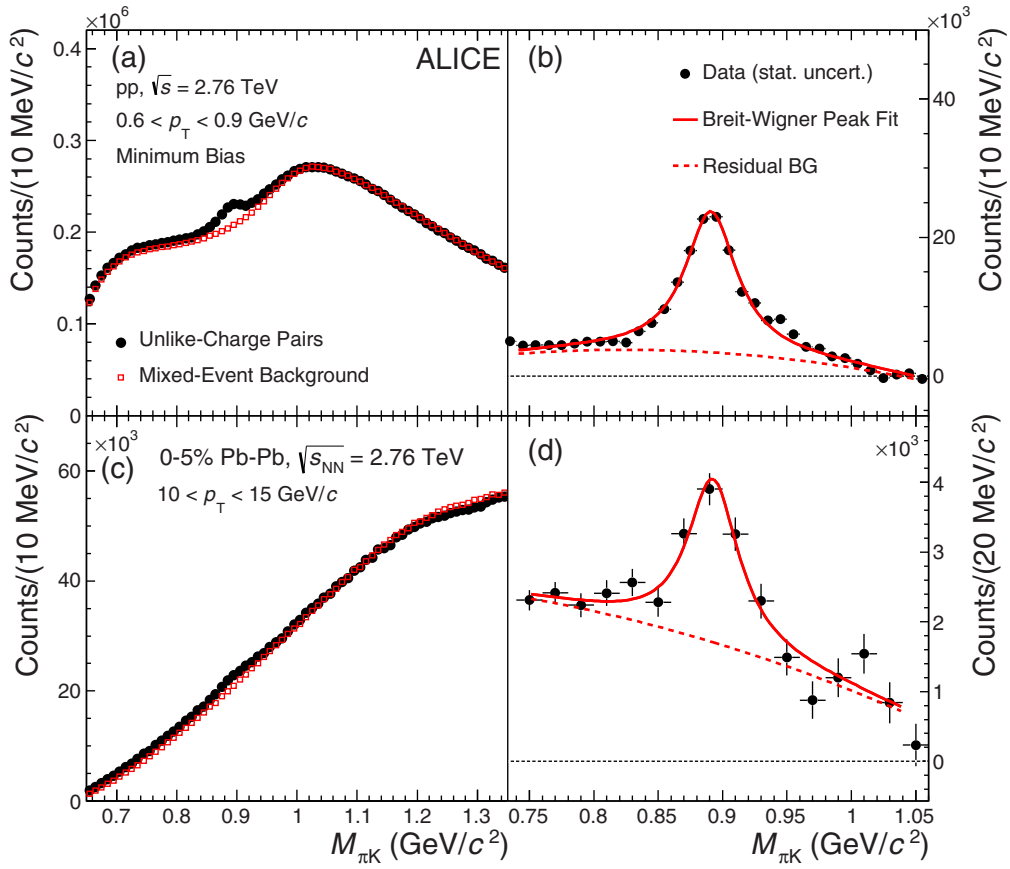

FIG. 1. Invariant-mass distributions of πK pairs for pp and the 0–5% most central Pb-Pb collisions at $\sqrt{s_{NN}} = 2.76$ TeV for the momentum ranges $0.6 < p_T < 0.9$ GeV/c (upper panel) and $10 < p_T < 15$ GeV/c (lower panel), respectively. Panels (a) and (c) show the unlike charge πK invariant-mass distribution from the same event and normalized mixed event background. Panels (b) and (d) report the invariant-mass distribution after subtraction of the combinatorial background for K^{*0}. The statistical uncertainties are shown by bars. The solid curves represent fits to the distributions and the red dashed curves are the components of those fits that describe the residual background.

of its daughters at the primary vertex. The invariant-mass distribution of the daughter pairs is constructed using all unlike-sign pairs of charged K candidates with oppositely charged π (K) candidates for K^{*0} (ϕ). The rapidity of πK and KK pairs is required to lie within the range $|y_{\text{pair}}| < 0.5$.

The signal extraction follows the procedure of the already published analysis [18]. The combinatorial background is estimated using the event mixing technique by pairing decay daughter candidates from two different events with similar primary vertex positions (v_z) and centrality percentiles in Pb-Pb collisions. For the K^{*0} analysis, the difference in the event plane angles between two events is required to be less than 30°. The Pb-Pb data sample is divided into 10 bins in centrality percentiles and 20 bins in v_z. Each event is mixed with 5 other similar events for both πK and KK. For event mixing in pp collisions, the binning takes into account the multiplicity of charged particles measured using the TPC. The total multiplicity and v_z are divided in 10 bins each for both πK and KK. These requirements ensure that the mixed events have similar features, so the invariant-mass distribution from the event mixing can better reproduce the combinatorial background.

In Fig. 1 (Fig. 2), panels (a) and (c) show the $\pi^{\mp}K^{\pm}$ (K^+K^-) invariant-mass distributions from the same event and mixed events for $0.6 < p_T < 0.9$ GeV/c ($0.5 < p_T < 0.8$ GeV/c) in minimum bias pp collisions and $10 < p_T < 15$ GeV/c ($10 < p_T < 13$ GeV/c) in 0–5% central Pb-Pb collisions at $\sqrt{s_{NN}} = 2.76$ TeV. The mixed event distribution is normalized to the same event distribution in the invariant-mass region of 1.1 to 1.3 GeV/c^2 (1.04 to 1.06 GeV/c^2), which is away from the signal peaks. The $\pi^{\mp}K^{\pm}$ (K^+K^-) invariant-mass distributions after mixed event background subtraction are shown in panels (b) and (d) of Fig. 1 (Fig. 2), where the signals are observed on top of a residual background. The residual background is due to correlated πK or KK pairs emitted within jets and from mis-reconstructed hadronic decays [18]. The shape of the residual background is studied by means of Monte Carlo simulations. It exhibits a smooth dependence on mass and a second-order polynomial is found to be a suitable function to describe the residual background for both K^{*0} and ϕ.

For each p_T interval and collision centrality class, the invariant-mass distribution is fitted with the sum of a peak fit function and a second-order polynomial to account for the residual background. The πK distribution signal peak is parametrized with a Breit-Wigner function. The fit function

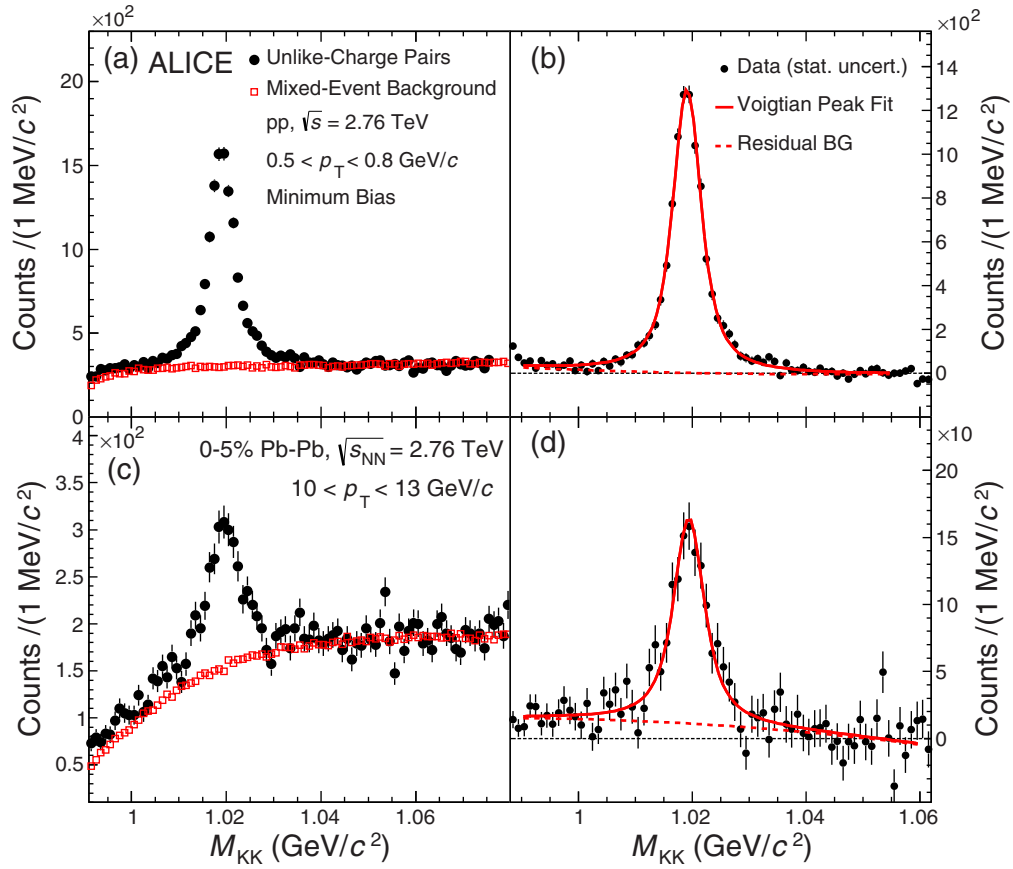

FIG. 2. Invariant-mass distributions of KK pairs for pp and the 0–5% most central Pb-Pb collisions at $\sqrt{s_{NN}} = 2.76$ TeV for the momentum ranges $0.5 < p_T < 0.8$ GeV/c (upper panel) and $10 < p_T < 13$ GeV/c (lower panel), respectively. In panels (a) and (c) the unlike charge KK invariant-mass distribution from the same event and normalized mixed event background are shown. In panels (b) and (d) the invariant-mass distribution after subtraction of the combinatorial background for ϕ is shown. The statistical uncertainties are shown by bars. The solid curves are the fits to the distributions and the red dashed curves are the components of those fits that describe the residual background.

for K^{*0} is

$$\frac{dN}{dm_{\pi K}} = \frac{Y}{2\pi} \times \frac{\Gamma_0}{(m_{\pi K} - M_0)^2 + \frac{\Gamma_0^2}{4}} + \left(Am_{\pi K}^2 + Bm_{\pi K} + C\right), \quad (2)$$

where M_0 is the reconstructed mass of K^{*0}, Γ_0 is the resonance width fixed to the value in vacuum [14], and Y is yield of the K^{*0} meson. The mass resolution of the K^{*0} is negligible compared to its width (47.4 ± 0.6 MeV/c^2) and is therefore not included in the K^{*0} fitting function. A, B, and C are the polynomial fit parameters. Similarly, the KK signal peak is fitted with a Voigtian function (a Breit-Wigner function convoluted with a Gaussian function), which accounts for the resonance width and the detector mass resolution. The fit function for ϕ is

$$\frac{dN}{dm_{KK}} = \frac{Y\Gamma_0}{(2\pi^{3/2})\sigma} \times \int_{-\infty}^{+\infty} \exp\left(\frac{(m_{KK} - m')^2}{2\sigma^2}\right) \times \frac{1}{(m' - M_0)^2 + \frac{\Gamma_0^2}{4}} dm' + \left(Am_{KK}^2 + Bm_{KK} + C\right), \quad (3)$$

where the parameter σ is the p_T-dependent mass resolution, which is found to be independent of collision centrality. For Pb-Pb (pp) collisions, the mass resolution parameter has been extracted by using HIJING (PYTHIA) [27,28] simulations, where the decay products of ϕ are propagated through the ALICE detector by using GEANT3 [29].

The $\pi^{\mp}K^{\pm}$ (K^+K^-) invariant-mass distribution is fitted in the range $0.75 < m_{\pi K} < 1.05$ GeV/c^2 ($0.99 < m_{KK} < 1.06$ GeV/c^2). The yield of K^{*0} (ϕ) is extracted in each p_T interval and centrality class by integrating the mixed-event background subtracted invariant-mass distribution in the range $0.77 < m_{\pi K} < 1.02$ GeV/c^2 ($1 < m_{KK} < 1.03$ GeV/c^2), subtracting the integral of the residual background function in the same range, and correcting the result to account for the yields outside this range. This correction to the total yield is about 9% (13%) for K^{*0} (ϕ) [18].

C. Yield correction

The raw yields of K^{*0} and ϕ mesons are normalized to the number of events and corrected for the branching ratio (BR) [14], the detector acceptance (A), and the reconstruction efficiency ($\varepsilon_{\rm rec}$).

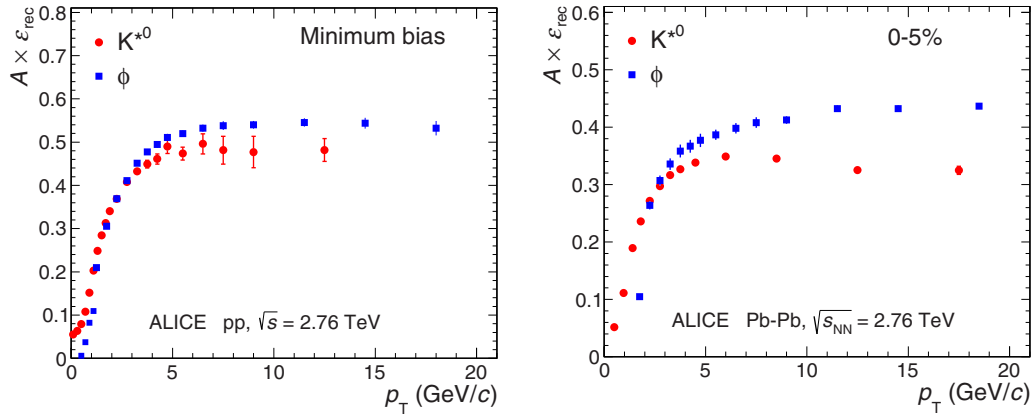

FIG. 3. The acceptance and efficiency ($A \times \varepsilon_{rec}$) correction as a function of p_T for K^{*0} (red marker) and ϕ (blue marker) mesons in pp (left panel) and 0–5% centrality in Pb-Pb (right panel) collisions at $\sqrt{s_{NN}} = 2.76$ TeV.

1. Acceptance and reconstruction efficiency

A Monte Carlo simulation based on the HIJING (PYTHIA) event generator is used for the estimation of the acceptance × efficiency ($A \times \varepsilon_{rec}$) in Pb-Pb ($pp$) collisions. Figure 3 shows $A \times \varepsilon_{rec}$ for minimum bias pp collisions and 0–5% centrality Pb-Pb collisions at $\sqrt{s_{NN}} = 2.76$ TeV for both K^{*0} and ϕ. In these simulations, the decay products of the generated K^{*0} and ϕ are propagated through the ALICE detector material using GEANT3 [29]. The $A \times \varepsilon_{rec}$ is defined as the fraction of generated K^{*0} and ϕ that is reconstructed after passing through the detector simulation, the event reconstruction, and being subjected to the track quality, PID, and pair rapidity cuts. In this calculation, only those K^{*0} (ϕ) mesons that decay to $K^{\pm}\pi^{\mp}$ (K^+K^-) are used. The correction for the branching ratio is therefore not included in $A \times \varepsilon_{rec}$ and is applied separately [Eq. (4)]. The differences in $A \times \varepsilon_{rec}$ for K^{*0} and ϕ are due to the different kinematics and track selection criteria. In Pb-Pb collisions, $A \times \varepsilon_{rec}$ has a very mild centrality dependence.

2. Normalization

The yields are normalized to the number of minimum bias events and corrected for the trigger ($\varepsilon_{trigger}$) and vertex reconstruction efficiencies (ε_{vertex}) to obtain the absolute resonance yields per inelastic pp collision. The ε_{vertex} correction was estimated to be equal to 89% and takes into account K^{*0} and ϕ meson losses after imposing the vertex cut. The trigger efficiency correction factor $\varepsilon_{trigger}$ is 88.1% with relative uncertainty of +5.9% and −3.5% for pp collisions [30]. The effects of trigger and vertex reconstruction efficiency corrections are negligible in Pb-Pb collisions and, hence, not considered. The invariant yield for pp and Pb-Pb collisions is

$$\frac{1}{2\pi p_T}\frac{d^2N}{dy\,dp_T} = \frac{1}{2\pi p_T} \times \frac{1}{N_{ev}} \times \frac{N^{raw}}{dy\,dp_T} \times \frac{\varepsilon_{trigger}}{A \times \varepsilon_{rec} \times BR \times \varepsilon_{vertex}}, \quad (4)$$

where N_{ev} is the number of events used in the analysis and N^{raw} is the K^{*0} or ϕ raw yield.

D. Systematic uncertainties

The sources of systematic uncertainties in the measurement of K^{*0} and ϕ production in pp and Pb-Pb collisions are the global tracking efficiency (performed using ITS and TPC clusters), track selection cuts, PID, yield extraction method, and material budget. In Pb-Pb (pp) collisions, the uncertainty contribution due to the global tracking efficiency has been estimated to be 5% (4%) for charged particles [31], which results in a 10% (8%) effect for the track pairs used for the invariant-mass analysis of K^{*0} and ϕ. The systematic uncertainty in the global tracking efficiency of the charged decay daughters is p_T and centrality independent and it cancels out partially in particle yield ratios for both K^{*0} and ϕ. The uncertainty due to the PID cuts is 3.7% (4%) in pp and 4% (6.2%) in Pb-Pb collisions for K^{*0} (ϕ). Systematic uncertainties of 3% to 6% on the raw yield have been assigned due to variation of the track selection cuts, depending on the particle species and collision system. The uncertainty due to the raw yield extraction includes variations of the fit range, fit function, mass resolution, and mixed event background normalization range. The πK (KK) invariant-mass fitting ranges were varied by 10–30 (5–10) MeV/c^2 on each side of the peak. The residual background is fitted with a third-order polynomial and the resulting variations in the raw yield are also incorporated into the systematic uncertainties. Due to the uncertainty in the material budget of the ALICE detectors, a systematic uncertainty of ≈1% (derived from the study for $\pi^{\pm}$ and $K^{\pm}$ in Ref. [31]) is added to the yield of K^{*0} and ϕ at low $p_T < 2$ GeV/c; the contribution is negligible at higher p_T. For ϕ the change in the yield due to a variation of the mass resolution is included in the systematic uncertainties of the raw yield extraction. The systematic uncertainties due to yield extraction are 2.5–14% (2–13%) for K^{*0} (ϕ) in pp collisions and 4–15% (3.5–13%) for K^{*0} (ϕ) in Pb-Pb collisions. Raw yield extraction dominates total uncertainties in the lowest and highest p_T intervals. All other systematic uncertainties have weak p_T and centrality dependence, with the exception of the yield extraction uncertainty. The total systematic uncertainties amount to 10–18% (9–16%) for K^{*0} (ϕ) in pp collisions and 12–19% (13–18%) for K^{*0} (ϕ) in Pb-Pb collisions. The contributions are summarized in Table II.

TABLE II. Systematic uncertainties in the measurement of K^{*0} and ϕ yields in pp and Pb-Pb collisions at $\sqrt{s_{NN}} = 2.76$ TeV. The global tracking uncertainty is p_{T} independent, while the other single valued systematic uncertainties are averaged over p_{T}. The values given in ranges are minimum and maximum uncertainties depending on p_{T} and centrality class. The normalization uncertainty, which is due to uncertainties in the boundaries of the centrality percentiles, is taken from [32].

Systematic variation	Pb-Pb		pp	
	K^{*0}	ϕ	K^{*0}	ϕ
Global tracking efficiency	10	10	8	8
Track selection	3–6	3–5	3	3
Particle identification	4.0	6.2	3.7	1–4
Material budget	<1	<1	0–3.3	0–3.3
Yield extraction	4–15	3.5–13	2.5–14	2–13
Total	12–19	13–18	10–18	9–16

III. RESULTS

A. p_{T} spectra in pp collisions

The first measurement of K^{*0} (ϕ) meson production in pp collisions at $\sqrt{s} = 2.76$ TeV up to $p_{\mathrm{T}} = 15$ (21) GeV/c is reported here. Figure 4 shows the transverse momentum spectra of K^{*0} and ϕ mesons in pp collisions at $\sqrt{s} = 2.76$ TeV, which are compared with the values given by perturbative QCD inspired Monte Carlo event generators PYTHIA [28,33] and PHOJET [34,35]. In both event generators hadronization is simulated using the Lund string fragmentation model [36]. Different PYTHIA tunes were developed by different groups through extensive comparison of Monte Carlo distributions with the minimum bias data from various experiments. The PYTHIA D6T tune [37] is adjusted to CDF Run 2 data, whereas the ATLAS-CSC tune [38] is adjusted using UA5, E375, and CDF data from $\sqrt{s} = 0.2$ to 1.8 TeV. The Perugia tune [39] uses the minimum bias and underlying event data from the LHC at 0.9 and 7 TeV. The bottom panels in Fig. 4 show the ratio of the model calculations to the data. For the K^{*0} meson, at low p_{T} (<1 GeV/c) all models overpredict the data. In the intermediate p_{T} range (≈2–8 GeV/c) the Perugia, ATLAS-CSC, and PYTHIA 8.14 tunes underestimate the data, the D6T tune overestimates the data, while PHOJET has good agreement with the data. For the ϕ meson, at low p_{T} (<1 GeV/c) PHOJET and the ATLAS-CSC tune overpredict, while the Perugia tune and PYTHIA 8.14 underpredict the data. In the intermediate p_{T} range (≈2–8 GeV/c) the Perugia tune, PYTHIA 8.14, and PHOJET underestimate the data, while the D6T and ATLAS-CSC tunes are in good agreement with the data. In the high p_{T} range (>8 GeV/c) all models agree with the data within the uncertainties for both K^{*0} and ϕ. For both K^{*0} and ϕ mesons, the deviations of these models from ALICE measurements are similar at both $\sqrt{s} = 2.76$ and 7 TeV [40].

B. p_{T} spectra in Pb-Pb collisions

Figure 5 shows the p_{T} spectra for K^{*0} and ϕ mesons for different centrality classes in Pb-Pb collisions at $\sqrt{s_{NN}} = 2.76$ TeV. The new measurements extend the previous results [18] from $p_{\mathrm{T}} = 5$ GeV/c to 20 (21) GeV/c for K^{*0} (ϕ). The production of K^{*0} has been measured in finer centrality bins and compared to previously published results [18]. When centrality bins are combined, the 2011 results are consistent with the 2010 data.

C. Particle ratios

The measurements of K^{*0} and ϕ spectra over a wide p_{T} range are used to probe particle production mechanisms at

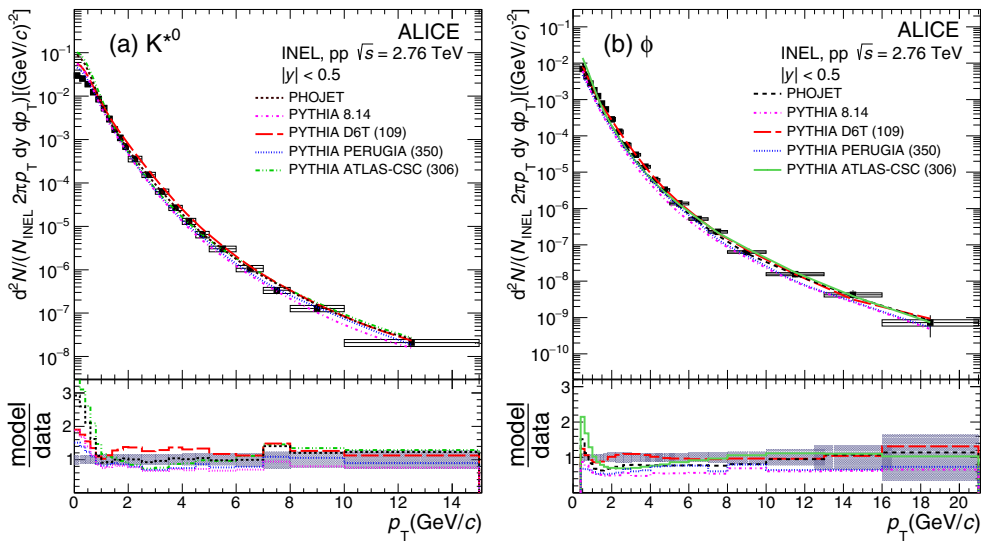

FIG. 4. Invariant yields for (a) K^{*0} and (b) ϕ mesons normalized to the number of inelastic pp collisions at $\sqrt{s} = 2.76$ TeV. Invariant yield is calculated by taking the value of p_{T} at the corresponding bin center. The statistical uncertainties on the data are shown by bars and the systematic uncertainties by boxes. The results are compared with model calculations from PYTHIA 8.14 [33], PHOJET [34,35], PYTHIA D6T [37], PYTHIA ATLAS-CSC [38], and PYTHIA Perugia [39] as shown by different dashed lines. The lower panel for both K^{*0} and ϕ shows the model-to-data ratio.

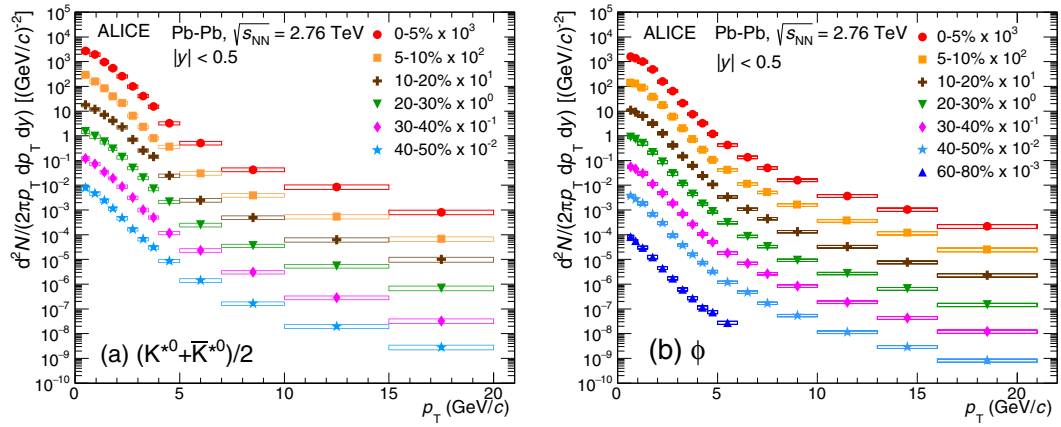

FIG. 5. Invariant yields of (a) K^{*0} and (b) ϕ mesons in various centrality classes in Pb-Pb collisions at $\sqrt{s_{NN}} = 2.76$ TeV. Invariant yield is calculated by taking the value of p_T at the corresponding bin center. The statistical and systematic uncertainties are shown as bars and boxes, respectively. The normalization uncertainty is not shown here, but is given in Table III.

different p_T scales. The p_T-integrated particle yield (dN/dy) and the mean transverse momentum ($\langle p_T \rangle$) have been extracted using the procedure described in Ref. [18]. The p_T distributions are fitted with a Lévy-Tsallis function [41,42] in pp and a Boltzmann-Gibbs blast-wave function [43] in Pb-Pb collisions. The dN/dy and $\langle p_T \rangle$ have been extracted from the data in the measured p_T region and the fit functions have been used to extrapolate into the unmeasured (low-p_T) region. The low-p_T extrapolation covers $p_T < 0.3$ (0.5) GeV/c for K^{*0} (ϕ) and accounts for 5% (14%) of the total yield. The yield is negligible at high-p_T (>20 GeV/c). These values for K^{*0} in pp and Pb-Pb collisions and the values for ϕ in pp collisions are listed in Table III.

Figure 6 shows the ratios K^{*0}/K^- and ϕ/K^- [18] as a function of $\langle dN_{ch}/d\eta \rangle^{1/3}$ (a proxy for the system size [44]) in Pb-Pb collisions at $\sqrt{s_{NN}} = 2.76$ TeV and pp collisions at $\sqrt{s} = 2.76$ TeV and 7 TeV [40]. The yield extraction dominates the systematic uncertainties at low p_T, and therefore in the integrated yield; it has been assumed to be fully uncorrelated between different centrality classes. The values of the K^{*0}/K^- ratio in Pb-Pb collisions at $\sqrt{s_{NN}} = 2.76$ TeV and pp collisions at $\sqrt{s} = 2.76$ TeV, along with ϕ/K^- ratio in pp collisions at $\sqrt{s} = 2.76$ TeV, are listed in Table III. The K^{*0}/K^- ratio from the present data is consistent with the trend observed in the previous measurement [18], also shown in Fig. 6 for completeness. A smooth dependence on $\langle dN_{ch}/d\eta \rangle^{1/3}$ is observed and the K^{*0}/K^- ratio is suppressed in the most central Pb-Pb collisions with respect to pp and peripheral Pb-Pb collisions. On the other hand, the ϕ/K^- ratio (previously reported in Ref. [18]) has weak centrality dependence without any suppression. Energy independence of the ϕ/K^- ratio in pp collisions is observed. The suppression of the integrated yield of the short-lived K^{*0} resonance suggests that the rescattering of its decay daughters in the hadronic medium reduces the measurable yield of K^{*0}. This aspect is further illustrated by comparison of the ratios to thermal model calculations with a chemical freeze-out temperature of 156 MeV [45]. The measurements of ϕ/K for the most central collisions agree with the thermal model expectation, while the measured K^{*0}/K ratio lies significantly below

TABLE III. The values of dN/dy, ratio to K^- [32] and $\langle p_T \rangle$ are presented for different centrality classes in Pb-Pb collisions and inelastic pp collisions. In each entry, the first uncertainty is statistical and the second is systematic, excluding the normalization uncertainty. Where a third uncertainty is given, it is the normalization uncertainty and the value in the parentheses corresponds to uncorrelated part of the systematic uncertainty.

K^{*0} (Pb-Pb $\sqrt{s_{NN}} = 2.76$ TeV)			
Centrality (%)	dN/dy	K^{*0}/K^-	$\langle p_T \rangle$ (GeV/c)
0–5	$19.56 \pm 0.93 \pm 2.48 \pm 0.097$	$0.180 \pm 0.008 \pm 0.026$ (0.023)	$1.310 \pm 0.023 \pm 0.055$
5–10	$16.71 \pm 0.65 \pm 2.08 \pm 0.083$	$0.186 \pm 0.007 \pm 0.026$ (0.024)	$1.252 \pm 0.023 \pm 0.055$
10–20	$13.65 \pm 0.63 \pm 1.84 \pm 0.009$	$0.200 \pm 0.009 \pm 0.026$ (0.023)	$1.360 \pm 0.026 \pm 0.053$
20–30	$10.37 \pm 0.50 \pm 1.38 \pm 0.010$	$0.225 \pm 0.011 \pm 0.025$ (0.023)	$1.322 \pm 0.028 \pm 0.053$
30–40	$7.35 \pm 0.28 \pm 0.97 \pm 0.146$	$0.245 \pm 0.009 \pm 0.025$ (0.021)	$1.254 \pm 0.023 \pm 0.050$
40–50	$4.66 \pm 0.20 \pm 0.65 \pm 0.111$	$0.258 \pm 0.011 \pm 0.025$ (0.022)	$1.220 \pm 0.025 \pm 0.050$
K^{*0} (pp $\sqrt{s} = 2.76$ TeV)			
Inelastic (INEL)	$0.0705 \pm 0.0007 \pm 0.009$	$0.307 \pm 0.003 \pm 0.043$	$0.950 \pm 0.005 \pm 0.026$
ϕ (pp $\sqrt{s} = 2.76$ TeV)			
	dN/dy	ϕ/K^-	$\langle p_T \rangle$ (GeV/c)
Inelastic (INEL)	$0.0260 \pm 0.0004 \pm 0.003$	$0.113 \pm 0.001 \pm 0.013$	$1.04 \pm 0.01 \pm 0.09$

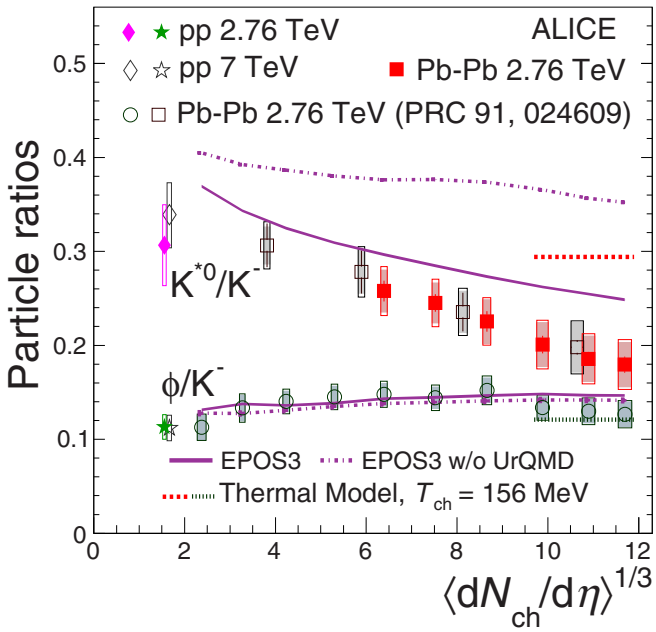

FIG. 6. K^{*0}/K^{-} and ϕ/K^{-} ratios as a function of $\langle dN_{\rm ch}/d\eta\rangle^{1/3}$ measured at mid-rapidity [44] in pp collisions at $\sqrt{s} = 2.76$ and 7 TeV [40], and Pb-Pb collisions at $\sqrt{s_{NN}} = 2.76$ TeV. For Pb-Pb collisions, the ϕ/K^{-} values are exclusively from [18]; the previously published K^{*0}/K^{-} measurements are compared to new measurements in finer centrality classes. Bars represent the statistical uncertainties, empty boxes represent the total systematic uncertainties, and shaded boxes represent the systematic uncertainties that are uncorrelated between centrality classes. The expectations from a thermal model calculation with a chemical freeze-out temperature of 156 MeV for the most central collisions [45] are shown. The EPOS3 calculation of the K^{*0}/K and ϕ/K ratios are also shown as a violet band for different centrality intervals [46].

the model value, as this thermal model does not include rescattering effects. The K^{*0}/K and ϕ/K ratios in Pb-Pb collisions are also compared to EPOS3 calculations [46]. EPOS3 is an event generator that describes the full evolution of heavy-ion collisions. The initial conditions are modeled using the Gribov-Regge multiple-scattering framework, based on strings and Pomerons. The collision volume is divided into two parts: a "core" (modeled as a QGP described by 3+1 dimensional viscous hydrodynamics) and a "corona" (where decaying strings are hadronized). The core is allowed to hadronize and the further evolution of the complete system (including rescattering and regeneration) is modeled using ultrarelativistic quantum molecular dynamics (UrQMD) [47,48]. EPOS3 with hadronic cascade modeled by UrQMD reproduces the observed trends for K^{*0}/K and ϕ/K ratios in Pb-Pb collisions, suggesting that the observed suppression of K^{*0}/K ratio is from rescattering of the daughter particles in the hadronic phase.

The effects of hadronic rescattering can be investigated with the $p_{\rm T}$-differential K^{*0}/K and ϕ/K ratios. Figure 7(a) shows the K^{*0}/K and ϕ/K ratios as a function of $p_{\rm T}$ in pp and 0–5% central Pb-Pb collisions at $\sqrt{s_{NN}} = 2.76$ TeV. For $p_{\rm T} < 2$ GeV/c, the K^{*0}/K ratio is smaller in central Pb-Pb collisions than in pp collisions, while the ϕ/K ratio is the same for both collision systems. This is consistent with the suppression of the K^{*0} yield due to rescattering in the hadronic phase. In Fig. 7(b), the K^{*0}/π and ϕ/π ratios are shown as a function of $p_{\rm T}$ in pp and 0–5% central Pb-Pb collisions at $\sqrt{s_{NN}} = 2.76$ TeV. For pp collisions, these ratios saturate at $p_{\rm T} \approx 4$ GeV/c, but in Pb-Pb collisions, they increase up to 4 GeV/c then show a decreasing trend up to 8 GeV/c, where finally they saturate. Both ratios in central Pb-Pb collisions show an enhancement with respect to pp collisions at $p_{\rm T} \approx 3$ GeV/c. Similar meson-to-meson enhancement has been observed for the K/π ratio [31], and is understood in terms of radial flow. The ratios K^{*0}/K, ϕ/K, K^{*0}/π, and ϕ/π are similar at high $p_{\rm T}$ (>8 GeV/c) in Pb-Pb and pp collisions. This suggests that fragmentation is the dominant mechanism of hadron production in this $p_{\rm T}$ regime. This observation is consistent with our previous measurements of the p/π and K/π ratios [31].

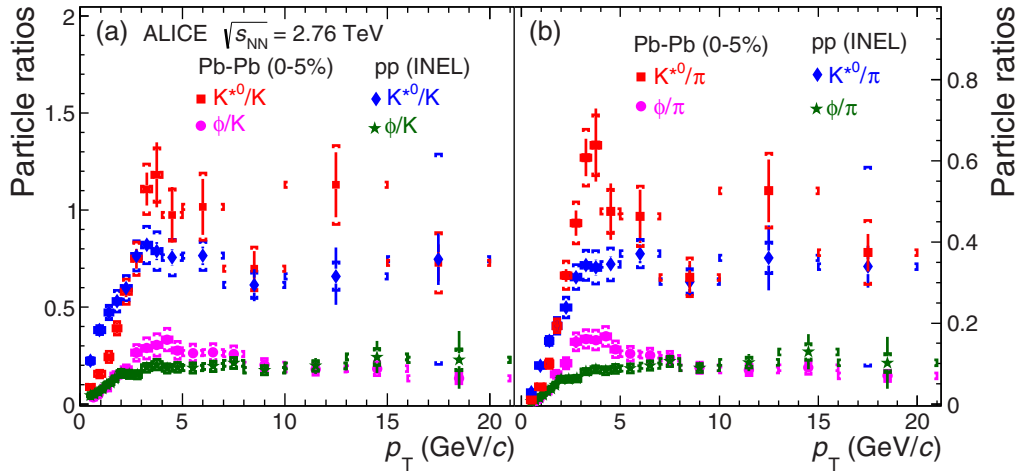

FIG. 7. Ratios of particle yields K^{*0}/K and ϕ/K in panel (a) and K^{*0}/π and ϕ/π in panel (b) as a function of $p_{\rm T}$ in central Pb-Pb and pp collisions at $\sqrt{s_{NN}} = 2.76$ TeV are shown. Here, $(K^{*0} + \overline{K}^{*0})$, $(K^{+} + K^{-})$, and $(\pi^{+} + \pi^{-})$ are denoted as K^{*0}, K, and π, respectively. The statistical and systematic uncertainties are shown as bars and caps respectively.

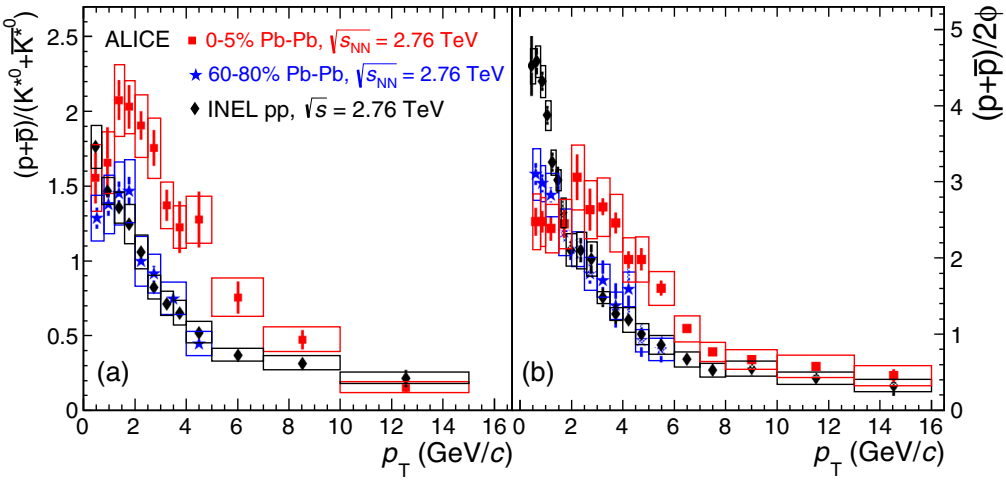

FIG. 8. Ratios of particle yields p/K^{*0} in panel (a) and p/ϕ in panel (b) as a function of p_T in central and peripheral Pb-Pb collisions and pp collisions at $\sqrt{s_{NN}} = 2.76$ TeV. The p/ϕ ratio for $p_T < 4$ GeV/c is from [18]. The statistical and systematic uncertainties are shown as bars and boxes respectively.

In Fig. 8, the p_T-differential p/K^{*0} and p/ϕ ratios measured in pp and Pb-Pb collisions at $\sqrt{s_{NN}} = 2.76$ TeV are shown in panels (a) and (b), respectively. The particle ratios evolve from pp to central Pb-Pb collisions, indicating a change of the spectral shapes. In central Pb-Pb collisions, the p/K^{*0} ratio shows weak transverse momentum dependence and the p/ϕ ratio is consistent with previous observations for $p_T \lesssim 4$ GeV/c. The similarity of the shapes of spectra for

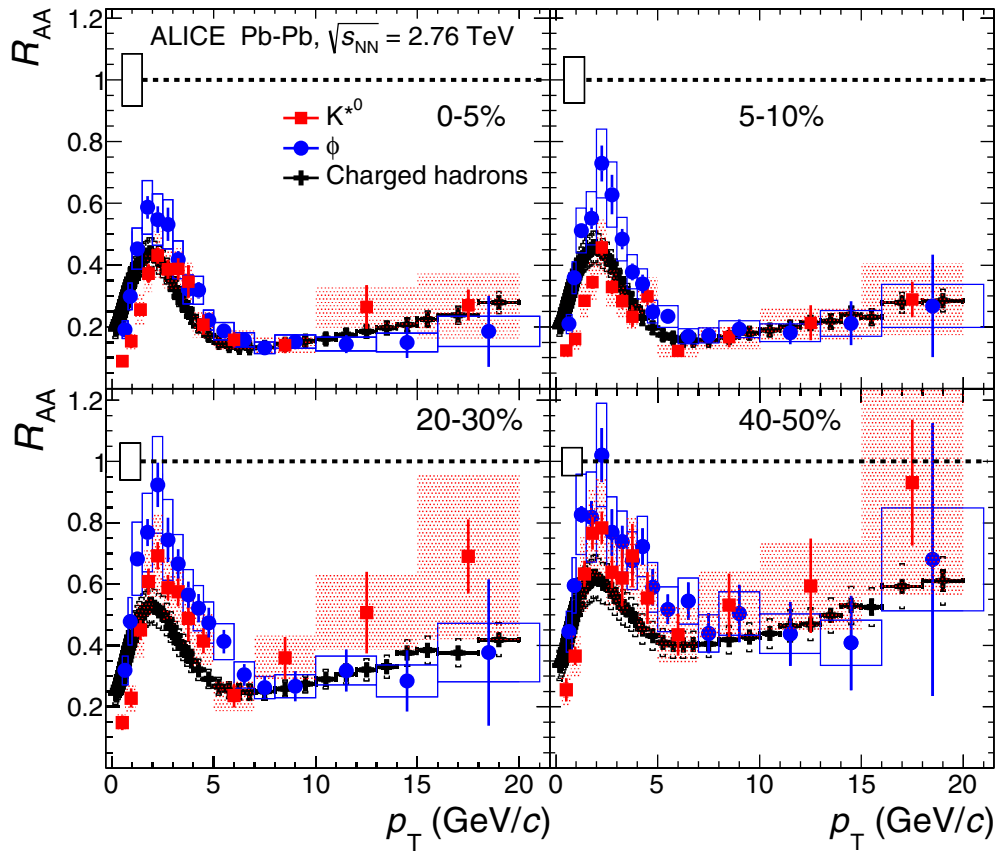

FIG. 9. The nuclear modification factor, R_{AA}, as a function of p_T for K^{*0} and ϕ mesons in Pb-Pb collisions for different centrality classes. The results are compared with the R_{AA} of charged hadrons measured by ALICE [50]. The statistical and systematic uncertainties are shown as bars and boxes, respectively. The boxes around unity indicate the uncertainty on the normalization of R_{AA}, including the uncertainty on the nuclear overlap function $\langle T_{AA} \rangle$ and the normalization uncertainty given in Table III.

K^{*0}, p, ϕ, which have similar masses but different numbers of valence quarks, suggests that the shapes are mostly defined by hadron masses, as expected from hydrodynamic models [49]. At higher p_{T}, the difference between particle ratios measured in different collision systems becomes smaller. Eventually the p/K^{*0} and p/ϕ ratios for $p_{\mathrm{T}} > 8$ GeV/c have similar values in both pp and central Pb-Pb collisions within uncertainties, as expected if parton fragmentation in vacuum dominates.

D. Nuclear modification factor (R_{AA})

The p_{T} spectrum of K^{*0} (ϕ) in pp collisions is used for the calculation of the nuclear modification factor (R_{AA}). The K^{*0} spectra are measured up to $p_{\mathrm{T}} = 15$ GeV/c (Fig. 4) and $p_{\mathrm{T}} = 20$ GeV/c (Fig. 5), in pp and Pb-Pb collisions, respectively. In pp collisions, the K^{*0} p_{T} distribution for $15 < p_{\mathrm{T}} < 20$ GeV/c is extrapolated from the measured data using a Lévy-Tsallis function [41,42]. For the systematic uncertainty on this extrapolated data point, a power-law function is used in the range $2 < p_{\mathrm{T}} < 20$ GeV/c. In addition, maximally hard and maximally soft p_{T} spectra are generated by shifting the measured data points within their uncertainties. The extrapolation procedure is performed on these hard and soft spectra and the changes in the high-p_{T} yield are incorporated into the systematic uncertainty estimate of the extrapolated data point.

The R_{AA} is used to study the effect of the medium formed in heavy-ion collisions and is sensitive to the system size and the density of the medium. The R_{AA} measurement is also sensitive to the dynamics of particle production, in-medium effects, and the energy loss mechanism of partons in the medium. If a nuclear collision were simply a superposition of nucleon-nucleon collisions, the nuclear modification factor would be equal to unity at high p_{T}. Deviations of R_{AA} from unity may indicate the presence of in-medium effects.

Figure 9 shows the R_{AA} of K^{*0} and ϕ in the 0–5% to 40–50% centrality classes for Pb-Pb collisions at $\sqrt{s_{NN}} = 2.76$ TeV. These results are compared to the R_{AA} of charged hadrons measured by the ALICE Collaboration [50]. The R_{AA} of K^{*0} and ϕ is lower than unity at high p_{T} (>8 GeV/c) for all centrality classes. It is also observed that for $p_{\mathrm{T}} < 2$ GeV/c, the K^{*0} R_{AA} is smaller than the ϕ and the charged hadron R_{AA}. This additional suppression of K^{*0} at low p_{T} with respect to ϕ is reduced as one goes from central to peripheral collisions, consistent with the expectation of more rescattering in central Pb-Pb collisions [18]. At high p_{T}, the R_{AA} of both K^{*0} and ϕ mesons are similar to that of charged hadrons and the R_{AA} values increase from central to peripheral collisions.

Figure 10 shows the comparison of R_{AA} of K^{*0} and ϕ in the 0–5% collision centrality class with that of π, K, and p [31]. In the intermediate p_{T} range (2–6 GeV/c), K^{*0} and ϕ R_{AA} are similar to that of the K, whereas p and ϕ exhibit a different trend despite similar masses. The difference of ϕ and p R_{AA} at RHIC was thought to be an effect of hadronization through parton recombination [51–53]. But the p/ϕ ratio in most central Pb-Pb collisions at LHC is observed to be flat for $p_{\mathrm{T}} < 4$ GeV/c (see also Fig. 8(b) and [18]) which suggests that particle masses determine the shapes of the p_{T} spectra with no need to invoke a recombination model. For $p_{\mathrm{T}} > 8$ GeV/c, all

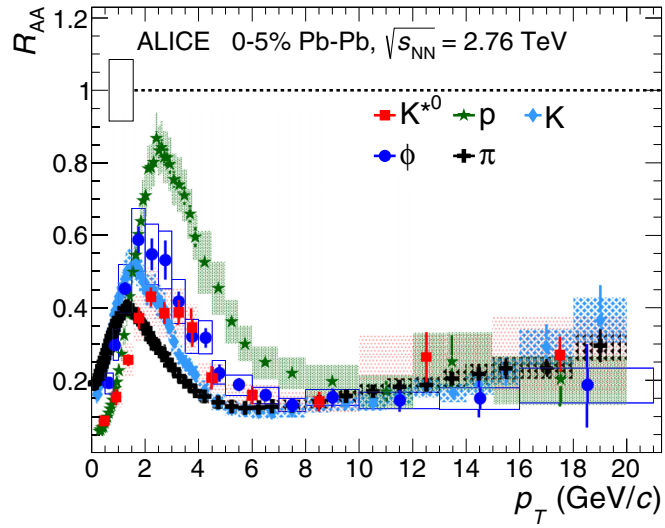

FIG. 10. The R_{AA} for K^{*0} and ϕ mesons as a function of p_{T} in 0–5% Pb-Pb collisions. The results are compared with the R_{AA} of π, K, and p [31]. The statistical and systematic uncertainties are shown as bars and boxes, respectively. The boxes around unity indicate the uncertainty on the normalization of R_{AA}, including the uncertainty on the nuclear overlap function $\langle T_{AA} \rangle$ and the normalization uncertainty given in Table III.

the light flavored species, π, K, p [31], K^{*0}, and ϕ show a similar suppression within uncertainties. This observation rules out models where the suppression of different species containing light quarks are considered to be dependent on their mass and it can also put a stringent constraint on the models dealing with fragmentation and energy loss mechanisms [8–10].

IV. CONCLUSIONS

The production of K^{*0} and ϕ mesons in inelastic pp collisions and Pb-Pb collisions in various centrality classes at $\sqrt{s_{NN}} = 2.76$ TeV using large data samples accumulated in 2011 has been measured. The transverse momentum distributions for K^{*0} (ϕ) mesons measured in pp collisions up to 15 (21) GeV/c are compared to predictions of the perturbative QCD inspired event generators PYTHIA and PHOJET. It is observed that for $p_{\mathrm{T}} > 8$ GeV/c the models agree with the data within uncertainties. In Pb-Pb collisions previously published results for K^{*0} and ϕ [18] are extended from $p_{\mathrm{T}} = 5$ to 20 GeV/c and the production of K^{*0} is studied in finer centrality bins. At high transverse momentum ($p_{\mathrm{T}} > 8$ GeV/c) nuclear modification factors for different light hadrons (π, K, K^{*0}, p, and ϕ) are consistent within uncertainties and particle ratios (K^{*0}/π, K^{*0}/K, ϕ/π, and ϕ/K) are similar for pp and Pb-Pb collisions. This indicates a particle species independence of partonic energy loss in the medium for light quark flavors (u,d,s) and points to fragmentation in vacuum as the dominant particle production mechanism in this kinematic regime. The K^{*0}/π and ϕ/π ratios show a centrality dependent enhancement at $p_{\mathrm{T}} \approx 3$ GeV/c in Pb-Pb collisions compared to pp collisions. This is similar to the enhancement previously observed in the K/π ratio [31] and attributed to

the development of collective radial flow. At low momentum, the production of K^{*0} is significantly suppressed in Pb-Pb collisions and the K^{*0}/K ratio exhibits suppression at low momentum, which increases with centrality. This observation is consistent with previous measurements by the STAR [54,55] and the ALICE [18] Collaborations and EPOS3 calculations [46], which confirms the importance of rescattering in the hadronic phase.

ACKNOWLEDGMENTS

The ALICE Collaboration would like to thank all its engineers and technicians for their invaluable contributions to the construction of the experiment and the CERN accelerator teams for the outstanding performance of the LHC complex. The ALICE Collaboration gratefully acknowledges the resources and support provided by all Grid centres and the Worldwide LHC Computing Grid (WLCG) collaboration. The ALICE Collaboration acknowledges the following funding agencies for their support in building and running the ALICE detector: A. I. Alikhanyan National Science Laboratory (Yerevan Physics Institute) Foundation (ANSL), State Committee of Science and World Federation of Scientists (WFS), Armenia; Austrian Academy of Sciences and Nationalstiftung für Forschung, Technologie und Entwicklung, Austria; Ministry of Communications and High Technologies, National Nuclear Research Center, Azerbaijan; Conselho Nacional de Desenvolvimento Científico e Tecnológico (CNPq), Universidade Federal do Rio Grande do Sul (UFRGS), Financiadora de Estudos e Projetos (Finep), and Fundação de Amparo à Pesquisa do Estado de São Paulo (FAPESP), Brazil; Ministry of Science and Technology of China (MSTC), National Natural Science Foundation of China (NSFC), and Ministry of Education of China (MOEC), China; Ministry of Science, Education and Sport and Croatian Science Foundation, Croatia; Ministry of Education, Youth and Sports of the Czech Republic, Czech Republic; The Danish Council for Independent Research - Natural Sciences, the Carlsberg Foundation, and Danish National Research Foundation (DNRF), Denmark; Helsinki Institute of Physics (HIP), Finland; Commissariat à l'Energie Atomique (CEA) and Institut National de Physique Nucléaire et de Physique des Particules (IN2P3) and Centre National de la Recherche Scientifique (CNRS), France; Bundesministerium für Bildung, Wissenschaft, Forschung und Technologie (BMBF) and GSI Helmholtzzentrum für Schwerionenforschung GmbH, Germany; Ministry of Education, Research and Religious Affairs, Greece; National Research, Development and Innovation Office, Hungary; Department of Atomic Energy Government of India (DAE) and Council of Scientific and Industrial Research (CSIR), New Delhi, India; Indonesian Institute of Science, Indonesia; Centro Fermi - Museo Storico della Fisica e Centro Studi e Ricerche Enrico Fermi and Istituto Nazionale di Fisica Nucleare (INFN), Italy; Institute for Innovative Science and Technology, Nagasaki Institute of Applied Science (IIST), Japan Society for the Promotion of Science (JSPS) KAKENHI, and Japanese Ministry of Education, Culture, Sports, Science and Technology (MEXT), Japan; Consejo Nacional de Ciencia (CONACYT) y Tecnología, through Fondo de Cooperación Internacional en Ciencia y Tecnología (FONCICYT) and Dirección General de Asuntos del Personal Academico (DGAPA), Mexico; Nationaal Instituut voor Subatomaire Fysica (Nikhef), Netherlands; The Research Council of Norway, Norway; Commission on Science and Technology for Sustainable Development in the South (COMSATS), Pakistan; Pontificia Universidad Católica del Perú, Peru; Ministry of Science and Higher Education and National Science Centre, Poland; Korea Institute of Science and Technology Information and National Research Foundation of Korea (NRF), Republic of Korea; Ministry of Education and Scientific Research, Institute of Atomic Physics and Romanian National Agency for Science, Technology and Innovation, Romania; Joint Institute for Nuclear Research (JINR), Ministry of Education and Science of the Russian Federation, and National Research Centre Kurchatov Institute, Russia; Ministry of Education, Science, Research and Sport of the Slovak Republic, Slovakia; National Research Foundation of South Africa, South Africa; Centro de Aplicaciones Tecnológicas y Desarrollo Nuclear (CEADEN), Cubaenergía, Cuba, Ministerio de Ciencia e Innovacion and Centro de Investigaciones Energéticas, Medioambientales y Tecnológicas (CIEMAT), Spain; Swedish Research Council (VR) and Knut and Alice Wallenberg Foundation (KAW), Sweden; European Organization for Nuclear Research, Switzerland; National Science and Technology Development Agency (NSDTA), Suranaree University of Technology (SUT), and Office of the Higher Education Commission under NRU project of Thailand, Thailand; Turkish Atomic Energy Agency (TAEK), Turkey; National Academy of Sciences of Ukraine, Ukraine; Science and Technology Facilities Council (STFC), United Kingdom; National Science Foundation of the United States of America (NSF) and United States Department of Energy, Office of Nuclear Physics (DOE NP), United States of America.

[1] J. Adams *et al.* (STAR Collaboration), Experimental and theoretical challenges in the search for the quark gluon plasma: The STAR Collaboration's critical assessment of the evidence from RHIC collisions, Nucl. Phys. A **757**, 102 (2005).

[2] K. Adcox *et al.* (PHENIX Collaboration), Formation of dense partonic matter in relativistic nucleus-nucleus collisions at RHIC: Experimental evaluation by the PHENIX collaboration, Nucl. Phys. A **757**, 184 (2005).

[3] M. Gyulassy and L. McLerran, New forms of QCD matter discovered at RHIC, Nucl. Phys. A **750**, 30 (2005).

[4] A. Adare *et al.* (PHENIX Collaboration), J/ψ Production versus Centrality, Transverse Momentum, and Rapidity in Au + Au Collisions at $\sqrt{s_{NN}} = 200$ GeV, Phys. Rev. Lett. **98**, 232301 (2007).

[5] A. Adare *et al.* (PHENIX Collaboration), J/ψ suppression at forward rapidity in Au + Au collisions at $\sqrt{s_{NN}} = 200$ GeV, Phys. Rev. C **84**, 054912 (2011).

[6] J. Adam *et al.* (ALICE Collaboration), Centrality dependence of high-p_T D meson suppression in Pb-Pb collisions at $\sqrt{s_{NN}} = 2.76$ TeV, J. High Energy Phys. 11 (2015) 205.

[7] J. Adam *et al.* (ALICE Collaboration), Transverse momentum dependence of D-meson production in Pb-Pb collisions at $\sqrt{s_{NN}} = 2.76$ TeV, J. High Energy Phys. 03 (2016) 081.

[8] R. Bellwied and C. Markert, In-medium hadronization in the deconfined matter at RHIC and LHC, Phys. Lett. B **691**, 208 (2010).

[9] W. Liu and R. J. Fries, Probing nuclear matter with jet conversions, Phys. Rev. C **77**, 054902 (2008).

[10] W. Liu, C. M. Ko, and B. W. Zhang, Jet conversions in a quark-gluon plasma, Phys. Rev. C **75**, 051901 (2007).

[11] M. Floris, Hadron yields and the phase diagram of strongly interacting matter, Nucl. Phys. A **931**, 103 (2014).

[12] S. Borsányi, Z. Fodor, C. Hoelbling, S. D. Katz, S. Krieg, C. Ratti, and K. K. Szabó (Wuppertal-Budapest Collaboration), Is there still any T_c mystery in lattice QCD? Results with physical masses in the continuum limit III, J. High Energy Phys. 09 (2010) 073.

[13] Y. Aoki, Z. Fodor, S. D. Katz, and K. K. Szabó, The QCD transition temperature: Results with physical masses in the continuum limit, Phys. Lett. B **643**, 46 (2006).

[14] K. A. Olive *et al.* (Particle Data Group), Review of Particle Physics, Chin. Phys. C **38**, 090001 (2014).

[15] G. Torrieri and J. Rafelski, Strange hadron resonances as a signature of freezeout dynamics, Phys. Lett. B **509**, 239 (2001).

[16] S. S. Adler *et al.* (PHENIX Collaboration), Scaling Properties of Proton and Antiproton Production in $\sqrt{s_{NN}} = 200$ GeV Au + Au Collisions, Phys. Rev. Lett. **91**, 172301 (2003).

[17] B. Abelev *et al.* (ALICE Collaboration), K^0_S and Λ Production in Pb-Pb Collisions at $\sqrt{s_{NN}} = 2.76$ TeV, Phys. Rev. Lett. **111**, 222301 (2013).

[18] B. Abelev *et al.* (ALICE Collaboration), $K^*(892)^0$ and $\phi(1020)$ production in Pb-Pb collisions at $\sqrt{s_{NN}} = 2.76$ TeV, Phys. Rev. C **91**, 024609 (2015).

[19] M. L. Miller, K. Reygers, S. J. Sanders, and P. Steinberg, Glauber modeling in high energy nuclear collisions, Annu. Rev. Nucl. Part. Sci. **57**, 205 (2007).

[20] B. Abelev *et al.* (ALICE Collaboration), Centrality determination of Pb-Pb collisions at $\sqrt{s_{NN}} = 2.76$ TeV with ALICE, Phys. Rev. C **88**, 044909 (2013).

[21] P. Cortese *et al.* (ALICE Collaboration), ALICE technical design report on forward detectors: FMD, T0 and V0, Report No. CERN-LHCC-2004-025, 2004 (unpublished).

[22] E. Abbas *et al.* (ALICE Collaboration), Performance of the ALICE VZERO system, J. Instrum. **8**, P10016 (2013).

[23] J. Adam *et al.* (ALICE Collaboration), Jet-like correlations with neutral pion triggers in *pp* and central Pb-Pb collisions at 2.76 TeV, Phys. Lett. B **763**, 238 (2016).

[24] P. Cortese *et al.* (ALICE Collaboration), ALICE: Physics performance report, volume II, J. Phys. G **32**, 1295 (2006).

[25] K. Aamodt *et al.* (ALICE Collaboration), The ALICE experiment at the CERN LHC, J. Instrum. **3**, S08002 (2008).

[26] B. Abelev *et al.* (ALICE Collaboration), Performance of the ALICE Experiment at the CERN LHC, Int. J. Mod. Phys. A **29**, 1430044 (2014).

[27] X.-N. Wang and M. Gyulassy, HIJING: A Monte Carlo model for multiple jet production in pp, pA, and AA collisions, Phys. Rev. D **44**, 3501 (1991).

[28] T. Sjöstrand, S. Mrenna, and P. Z. Skands, PYTHIA 6.4 physics and manual, J. High Energy Phys. 05 (2006) 026.

[29] R. Brun, F. Bruyant, F. Carminati, S. Giani, M. Maire *et al.*, GEANT detector description and simulation tool, Report No. CERN-W5013, 1994 (unpublished).

[30] B. Abelev *et al.* (ALICE Collaboration), Measurement of inelastic, single- and double-diffraction cross sections in proton–proton collisions at the LHC with ALICE, Eur. Phys. J. C **73**, 2456 (2013).

[31] B. Abelev *et al.* (ALICE Collaboration), Production of charged pions, kaons and protons at large transverse momenta in *pp* and Pb-Pb collisions at $\sqrt{s_{NN}} = 2.76$ TeV, Phys. Lett. B **736**, 196 (2014).

[32] B. Abelev *et al.* (ALICE Collaboration), Centrality dependence of π, K, and p production in Pb-Pb collisions at $\sqrt{s_{NN}} = 2.76$ TeV, Phys. Rev. C **88**, 044910 (2013).

[33] T. Sjöstrand, S. Mrenna, and P. Z. Skands, A brief introduction to PYTHIA 8.1, Comput. Phys. Commun. **178**, 852 (2008).

[34] R. Engel, Photoproduction within the two component dual parton model: Amplitudes and cross-sections, Z. Phys. C **66**, 203 (1995).

[35] R. Engel and J. Ranft, Hadronic photon-photon interactions at high-energies, Phys. Rev. D **54**, 4244 (1996).

[36] B. Andersson, G. Gustafson, G. Ingelman, and T. Sjöstrand, Parton fragmentation and string dynamics, Phys. Rep. **97**, 31 (1983).

[37] R. Field, Physics at the Tevatron, Acta Phys. Pol. B **39**, 2611 (2008).

[38] C. M. Buttar, D. Clements, I. Dawson, and A. Moraes, Simulations of minimum bias events and the underlying event, MC tuning and predictions for the LHC, Acta Phys. Pol. B **35**, 433 (2004).

[39] P. Z. Skands, Tuning Monte Carlo generators: The Perugia tunes, Phys. Rev. D **82**, 074018 (2010).

[40] B. Abelev *et al.* (ALICE Collaboration), Production of $K^*(892)^0$ and $\phi(1020)$ in *pp* collisions at $\sqrt{s} = 7$ TeV, Eur. Phys. J. C **72**, 2183 (2012).

[41] C. Tsallis, Possible generalization of Boltzmann-Gibbs statistics, J. Stat. Phys. **52**, 479 (1988).

[42] B. I. Abelev *et al.* (STAR Collaboration), Strange particle production in $p + p$ collisions at $\sqrt{s_{NN}} = 200$ GeV, Phys. Rev. C **75**, 064901 (2007).

[43] E. Schnedermann, J. Sollfrank, and U. W. Heinz, Thermal phenomenology of hadrons from 200A GeV S + S collisions, Phys. Rev. C **48**, 2462 (1993).

[44] K. Aamodt *et al.* (ALICE Collaboration), Two-pion Bose-Einstein correlations in central Pb-Pb collisions at $\sqrt{s_{NN}} = 2.76$ TeV, Phys. Lett. B **696**, 328 (2011).

[45] J. Stachel, A. Andronic, P. Braun-Munzinger, and K. Redlich, Confronting LHC data with the statistical hadronization model, J. Phys. Conf. Ser. **509**, 012019 (2014).

[46] A. G. Knospe, C. Markert, K. Werner, J. Steinheimer, and M. Bleicher, Hadronic resonance production and interaction in partonic and hadronic matter in the EPOS3 model with and without the hadronic afterburner UrQMD, Phys. Rev. C **93**, 014911 (2016).

[47] S. A. Bass *et al.*, Microscopic models for ultrarelativistic heavy ion collisions, Prog. Part. Nucl. Phys. **41**, 255 (1998).

[48] M. Bleicher *et al.*, Relativistic hadron hadron collisions in the ultrarelativistic quantum molecular dynamics model, J. Phys. G **25**, 1859 (1999).

[49] C. Shen, U. Heinz, P. Huovinen, and H. Song, Radial and elliptic flow in Pb + Pb collisions at the Large Hadron

Collider from viscous hydrodynamic, Phys. Rev. C **84**, 044903 (2011).

[50] B. Abelev *et al.* (ALICE Collaboration), Centrality dependence of charged particle production at large transverse momentum in Pb-Pb collisions at $\sqrt{s_{NN}} = 2.76$ TeV, Phys. Lett. B **720**, 52 (2013).

[51] A. Adare *et al.* (PHENIX Collaboration), Nuclear modification factors of ϕ mesons in $d+$Au, Cu + Cu, and Au + Au collisions at $\sqrt{s_{NN}} = 200$ GeV, Phys. Rev. C **83**, 024909 (2011).

[52] J. Ma, ϕ meson production in $\sqrt{s_{NN}} = 200$ GeV Au + Au and pp collisions at RHIC, J. Phys. G **30**, S543 (2004).

[53] G. Agakishiev *et al.* (STAR Collaboration), Identified Hadron Compositions in $p+p$ and Au + Au Collisions at High Transverse Momenta at $\sqrt{s_{NN}} = 200$ GeV, Phys. Rev. Lett. **108**, 072302 (2012).

[54] J. Adams *et al.* (STAR Collaboration), $K^*(892)^0$ resonance production in Au + Au and $p+p$ collisions at $\sqrt{s_{NN}} = 200$ GeV at STAR, Phys. Rev. C **71**, 064902 (2005).

[55] M. M. Aggarwal *et al.* (STAR Collaboration), K^{*0} production in Cu + Cu and Au + Au collisions at $\sqrt{s_{NN}} = 62.4$ GeV and 200 GeV, Phys. Rev. C **84**, 034909 (2011).

J. Adam,[38] D. Adamová,[87] M. M. Aggarwal,[91] G. Aglieri Rinella,[34] M. Agnello,[30,113] N. Agrawal,[47] Z. Ahammed,[139] S. Ahmad,[17] S. U. Ahn,[69] S. Aiola,[143] A. Akindinov,[54] S. N. Alam,[139] D. S. D. Albuquerque,[124] D. Aleksandrov,[83] B. Alessandro,[113] D. Alexandre,[104] R. Alfaro Molina,[64] A. Alici,[12,107] A. Alkin,[3] J. Alme,[21,36] T. Alt,[41] S. Altinpinar,[21] I. Altsybeev,[138] C. Alves Garcia Prado,[123] M. An,[7] C. Andrei,[80] H. A. Andrews,[104] A. Andronic,[100] V. Anguelov,[96] C. Anson,[90] T. Antičić,[101] F. Antinori,[110] P. Antonioli,[107] R. Anwar,[126] L. Aphecetche,[116] H. Appelshäuser,[60] S. Arcelli,[26] R. Arnaldi,[113] O. W. Arnold,[97,35] I. C. Arsene,[20] M. Arslandok,[60] B. Audurier,[116] A. Augustinus,[34] R. Averbeck,[100] M. D. Azmi,[17] A. Badalà,[109] Y. W. Baek,[68] S. Bagnasco,[113] R. Bailhache,[60] R. Bala,[93] A. Baldisseri,[65] M. Ball,[44] R. C. Baral,[57] A. M. Barbano,[25] R. Barbera,[27] F. Barile,[32] L. Barioglio,[25] G. G. Barnaföldi,[142] L. S. Barnby,[104,34] V. Barret,[71] P. Bartalini,[7] K. Barth,[34] J. Bartke,[120,*] E. Bartsch,[60] M. Basile,[26] N. Bastid,[71] S. Basu,[139] B. Bathen,[61] G. Batigne,[116] A. Batista Camejo,[71] B. Batyunya,[67] P. C. Batzing,[20] I. G. Bearden,[84] H. Beck,[96] C. Bedda,[30] N. K. Behera,[50] I. Belikov,[135] F. Bellini,[26] H. Bello Martinez,[2] R. Bellwied,[126] L. G. E. Beltran,[122] V. Belyaev,[76] G. Bencedi,[142] S. Beole,[25] A. Bercuci,[80] Y. Berdnikov,[89] D. Berenyi,[142] R. A. Bertens,[53,129] D. Berzano,[34] L. Betev,[34] A. Bhasin,[93] I. R. Bhat,[93] A. K. Bhati,[91] B. Bhattacharjee,[43] J. Bhom,[120] L. Bianchi,[126] N. Bianchi,[73] C. Bianchin,[141] J. Bielčík,[38] J. Bielčíková,[87] A. Bilandzic,[35,97] G. Biro,[142] R. Biswas,[4] S. Biswas,[4] J. T. Blair,[121] D. Blau,[83] C. Blume,[60] G. Boca,[136] F. Bock,[75,96] A. Bogdanov,[76] L. Boldizsár,[142] M. Bombara,[39] G. Bonomi,[137] M. Bonora,[34] J. Book,[60] H. Borel,[65] A. Borissov,[99] M. Borri,[128] E. Botta,[25] C. Bourjau,[84] P. Braun-Munzinger,[100] M. Bregant,[123] T. A. Broker,[60] T. A. Browning,[98] M. Broz,[38] E. J. Brucken,[45] E. Bruna,[113] G. E. Bruno,[32] D. Budnikov,[102] H. Buesching,[60] S. Bufalino,[30,25] P. Buhler,[115] S. A. I. Buitron,[62] P. Buncic,[34] O. Busch,[132] Z. Buthelezi,[66] J. B. Butt,[15] J. T. Buxton,[18] J. Cabala,[118] D. Caffarri,[34] H. Caines,[143] A. Caliva,[53] E. Calvo Villar,[105] P. Camerini,[24] A. A. Capon,[115] F. Carena,[34] W. Carena,[34] F. Carnesecchi,[26,12] J. Castillo Castellanos,[65] A. J. Castro,[129] E. A. R. Casula,[23,108] C. Ceballos Sanchez,[9] P. Cerello,[113] J. Cerkala,[118] B. Chang,[127] S. Chapeland,[34] M. Chartier,[128] J. L. Charvet,[65] S. Chattopadhyay,[139] S. Chattopadhyay,[103] A. Chauvin,[97,35] M. Cherney,[90] C. Cheshkov,[134] B. Cheynis,[134] V. Chibante Barroso,[34] D. D. Chinellato,[124] S. Cho,[50] P. Chochula,[34] K. Choi,[99] M. Chojnacki,[84] S. Choudhury,[139] P. Christakoglou,[85] C. H. Christensen,[84] P. Christiansen,[33] T. Chujo,[132] S. U. Chung,[99] C. Cicalo,[108] L. Cifarelli,[12,26] F. Cindolo,[107] J. Cleymans,[92] F. Colamaria,[32] D. Colella,[55,34] A. Collu,[75] M. Colocci,[26] G. Conesa Balbastre,[72] Z. Conesa del Valle,[51] M. E. Connors,[143,†] J. G. Contreras,[38] T. M. Cormier,[88] Y. Corrales Morales,[113] I. Cortés Maldonado,[2] P. Cortese,[31] M. R. Cosentino,[125] F. Costa,[34] S. Costanza,[136] J. Crkovská,[51] P. Crochet,[71] R. Cruz Albino,[11] E. Cuautle,[62] L. Cunqueiro,[61] T. Dahms,[35,97] A. Dainese,[110] M. C. Danisch,[96] A. Danu,[58] D. Das,[103] I. Das,[103] S. Das,[4] A. Dash,[81] S. Dash,[47] S. De,[48,123] A. De Caro,[29] G. de Cataldo,[106] C. de Conti,[123] J. de Cuveland,[41] A. De Falco,[23] D. De Gruttola,[12,29] N. De Marco,[113] S. De Pasquale,[29] R. D. De Souza,[124] H. F. Degenhardt,[123] A. Deisting,[100,96] A. Deloff,[79] C. Deplano,[85] P. Dhankher,[47] D. Di Bari,[32] A. Di Mauro,[34] P. Di Nezza,[73] B. Di Ruzza,[110] M. A. Diaz Corchero,[10] T. Dietel,[92] P. Dillenseger,[60] R. Divià,[34] Ø. Djuvsland,[21] A. Dobrin,[58,34] D. Domenicis Gimenez,[123] B. Dönigus,[60] O. Dordic,[20] T. Drozhzhova,[60] A. K. Dubey,[139] A. Dubla,[100] L. Ducroux,[134] A. K. Duggal,[91] P. Dupieux,[71] R. J. Ehlers,[143] D. Elia,[106] E. Endress,[105] H. Engel,[59] E. Epple,[143] B. Erazmus,[116] F. Erhardt,[133] B. Espagnon,[51] S. Esumi,[132] G. Eulisse,[34] J. Eum,[99] D. Evans,[104] S. Evdokimov,[114] L. Fabbietti,[35,97] D. Fabris,[110] J. Faivre,[72] A. Fantoni,[73] M. Fasel,[88,75] L. Feldkamp,[61] A. Feliciello,[113] G. Feofilov,[138] J. Ferencei,[87] A. Fernández Téllez,[2] E. G. Ferreiro,[16] A. Ferretti,[25] A. Festanti,[28] V. J. G. Feuillard,[71,65] J. Figiel,[120] M. A. S. Figueredo,[123] S. Filchagin,[102] D. Finogeev,[52] F. M. Fionda,[23] E. M. Fiore,[32] M. Floris,[34] S. Foertsch,[66] P. Foka,[100] S. Fokin,[83] E. Fragiacomo,[112] A. Francescon,[34] A. Francisco,[116] U. Frankenfeld,[100] G. G. Fronze,[25] U. Fuchs,[34] C. Furget,[72] A. Furs,[52] M. Fusco Girard,[29] J. J. Gaardhøje,[84] M. Gagliardi,[25] A. M. Gago,[105] K. Gajdosova,[84] M. Gallio,[25] C. D. Galvan,[122] D. R. Gangadharan,[75] P. Ganoti,[78] C. Gao,[7] C. Garabatos,[100] E. Garcia-Solis,[13] K. Garg,[27] P. Garg,[48] C. Gargiulo,[34] P. Gasik,[35,97] E. F. Gauger,[121] M. B. Gay Ducati,[63] M. Germain,[116] P. Ghosh,[139] S. K. Ghosh,[4] P. Gianotti,[73] P. Giubellino,[34,113] P. Giubilato,[28] E. Gladysz-Dziadus,[120] P. Glässel,[96] D. M. Goméz Coral,[64] A. Gomez Ramirez,[59] A. S. Gonzalez,[34] V. Gonzalez,[10] P. González-Zamora,[10] S. Gorbunov,[41] L. Görlich,[120] S. Gotovac,[119] V. Grabski,[64] L. K. Graczykowski,[140] K. L. Graham,[104] L. Greiner,[75] A. Grelli,[53] C. Grigoras,[34] V. Grigoriev,[76] A. Grigoryan,[1]

S. Grigoryan,[67] N. Grion,[112] J. M. Gronefeld,[100] F. Grosa,[30] J. F. Grosse-Oetringhaus,[34] R. Grosso,[100] L. Gruber,[115] F. R. Grull,[59] F. Guber,[52] R. Guernane,[34,72] B. Guerzoni,[26] K. Gulbrandsen,[84] T. Gunji,[131] A. Gupta,[93] R. Gupta,[93] I. B. Guzman,[2] R. Haake,[34,61] C. Hadjidakis,[51] H. Hamagaki,[77,131] G. Hamar,[142] J. C. Hamon,[135] J. W. Harris,[143] A. Harton,[13] D. Hatzifotiadou,[107] S. Hayashi,[131] S. T. Heckel,[60] E. Hellbär,[60] H. Helstrup,[36] A. Herghelegiu,[80] G. Herrera Corral,[11] F. Herrmann,[61] B. A. Hess,[95] K. F. Hetland,[36] H. Hillemanns,[34] B. Hippolyte,[135] J. Hladky,[56] D. Horak,[38] R. Hosokawa,[132] P. Hristov,[34] C. Hughes,[129] T. J. Humanic,[18] N. Hussain,[43] T. Hussain,[17] D. Hutter,[41] D. S. Hwang,[19] R. Ilkaev,[102] M. Inaba,[132] M. Ippolitov,[83,76] M. Irfan,[17] V. Isakov,[52] M. S. Islam,[48] M. Ivanov,[34,100] V. Ivanov,[89] V. Izucheev,[114] B. Jacak,[75] N. Jacazio,[26] P. M. Jacobs,[75] M. B. Jadhav,[47] S. Jadlovska,[118] J. Jadlovsky,[118] C. Jahnke,[35] M. J. Jakubowska,[140] M. A. Janik,[140] P. H. S. Y. Jayarathna,[126] C. Jena,[81] S. Jena,[126] M. Jercic,[133] R. T. Jimenez Bustamante,[100] P. G. Jones,[104] A. Jusko,[104] P. Kalinak,[55] A. Kalweit,[34] J. H. Kang,[144] V. Kaplin,[76] S. Kar,[139] A. Karasu Uysal,[70] O. Karavichev,[52] T. Karavicheva,[52] L. Karayan,[100,96] E. Karpechev,[52] U. Kebschull,[59] R. Keidel,[145] D. L. D. Keijdener,[53] M. Keil,[34] B. Ketzer,[44] M. Mohisin Khan,[17,‡] P. Khan,[103] S. A. Khan,[139] A. Khanzadeev,[89] Y. Kharlov,[114] A. Khatun,[17] A. Khuntia,[48] M. M. Kielbowicz,[120] B. Kileng,[36] D. W. Kim,[42] D. J. Kim,[127] D. Kim,[144] H. Kim,[144] J. S. Kim,[42] J. Kim,[96] M. Kim,[50] M. Kim,[144] S. Kim,[19] T. Kim,[144] S. Kirsch,[41] I. Kisel,[41] S. Kiselev,[54] A. Kisiel,[140] G. Kiss,[142] J. L. Klay,[6] C. Klein,[60] J. Klein,[34] C. Klein-Bösing,[61] S. Klewin,[96] A. Kluge,[34] M. L. Knichel,[96] A. G. Knospe,[126] C. Kobdaj,[117] M. Kofarago,[34] T. Kollegger,[100] A. Kolojvari,[138] V. Kondratiev,[138] N. Kondratyeva,[76] E. Kondratyuk,[114] A. Konevskikh,[52] M. Kopcik,[118] M. Kour,[93] C. Kouzinopoulos,[34] O. Kovalenko,[79] V. Kovalenko,[138] M. Kowalski,[120] G. Koyithatta Meethaleveedu,[47] I. Králik,[55] A. Kravčáková,[39] M. Krivda,[55,104] F. Krizek,[87] E. Kryshen,[89] M. Krzewicki,[41] A. M. Kubera,[18] V. Kučera,[87] C. Kuhn,[135] P. G. Kuijer,[85] A. Kumar,[93] J. Kumar,[47] L. Kumar,[91] S. Kumar,[47] S. Kundu,[81] P. Kurashvili,[79] A. Kurepin,[52] A. B. Kurepin,[52] A. Kuryakin,[102] S. Kushpil,[87] M. J. Kweon,[50] Y. Kwon,[144] S. L. La Pointe,[41] P. La Rocca,[27] C. Lagana Fernandes,[123] I. Lakomov,[34] R. Langoy,[40] K. Lapidus,[143] C. Lara,[59] A. Lardeux,[20,65] A. Lattuca,[25] E. Laudi,[34] R. Lavicka,[38] L. Lazaridis,[34] R. Lea,[24] L. Leardini,[96] S. Lee,[144] F. Lehas,[85] S. Lehner,[115] J. Lehrbach,[41] R. C. Lemmon,[86] V. Lenti,[106] E. Leogrande,[53] I. León Monzón,[122] P. Lévai,[142] S. Li,[7] X. Li,[14] J. Lien,[40] R. Lietava,[104] S. Lindal,[20] V. Lindenstruth,[41] C. Lippmann,[100] M. A. Lisa,[18] V. Litichevskyi,[45] H. M. Ljunggren,[33] W. J. Llope,[141] D. F. Lodato,[53] P. I. Loenne,[21] V. Loginov,[76] C. Loizides,[75] P. Loncar,[119] X. Lopez,[71] E. López Torres,[9] A. Lowe,[142] P. Luettig,[60] M. Lunardon,[28] G. Luparello,[24] M. Lupi,[34] T. H. Lutz,[143] A. Maevskaya,[52] M. Mager,[34] S. Mahajan,[93] S. M. Mahmood,[20] A. Maire,[135] R. D. Majka,[143] M. Malaev,[89] I. Maldonado Cervantes,[62] L. Malinina,[67,§] D. Mal'Kevich,[54] P. Malzacher,[100] A. Mamonov,[102] V. Manko,[83] F. Manso,[71] V. Manzari,[106] Y. Mao,[7] M. Marchisone,[66,130] J. Mareš,[56] G. V. Margagliotti,[24] A. Margotti,[107] J. Margutti,[53] A. Marín,[100] C. Markert,[121] M. Marquard,[60] N. A. Martin,[100] P. Martinengo,[34] J. A. L. Martinez,[59] M. I. Martínez,[2] G. Martínez García,[116] M. Martinez Pedreira,[34] A. Mas,[123] S. Masciocchi,[100] M. Masera,[25] A. Masoni,[108] A. Mastroserio,[32] A. M. Mathis,[97,35] A. Matyja,[120,129] C. Mayer,[120] J. Mazer,[129] M. Mazzilli,[32] M. A. Mazzoni,[111] F. Meddi,[22] Y. Melikyan,[76] A. Menchaca-Rocha,[64] E. Meninno,[29] J. Mercado Pérez,[96] M. Meres,[37] S. Mhlanga,[92] Y. Miake,[132] M. M. Mieskolainen,[45] D. Mihaylov,[97] K. Mikhaylov,[67,54] L. Milano,[75] J. Milosevic,[20] A. Mischke,[53] A. N. Mishra,[48] T. Mishra,[57] D. Miśkowiec,[100] J. Mitra,[139] C. M. Mitu,[58] N. Mohammadi,[53] B. Mohanty,[81] E. Montes,[10] D. A. Moreira De Godoy,[61] L. A. P. Moreno,[2] S. Moretto,[28] A. Morreale,[116] A. Morsch,[34] V. Muccifora,[73] E. Mudnic,[119] D. Mühlheim,[61] S. Muhuri,[139] M. Mukherjee,[139] J. D. Mulligan,[143] M. G. Munhoz,[123] K. Münning,[44] R. H. Munzer,[35,97,60] H. Murakami,[131] S. Murray,[66] L. Musa,[34] J. Musinsky,[55] C. J. Myers,[126] B. Naik,[47] R. Nair,[79] B. K. Nandi,[47] R. Nania,[107] E. Nappi,[106] M. U. Naru,[15] H. Natal da Luz,[123] C. Nattrass,[129] S. R. Navarro,[2] K. Nayak,[81] R. Nayak,[47] T. K. Nayak,[139] S. Nazarenko,[102] A. Nedosekin,[54] R. A. Negrao De Oliveira,[34] L. Nellen,[62] S. V. Nesbo,[36] F. Ng,[126] M. Nicassio,[100] M. Niculescu,[58] J. Niedziela,[34] B. S. Nielsen,[84] S. Nikolaev,[83] S. Nikulin,[83] V. Nikulin,[89] F. Noferini,[107,12] P. Nomokonov,[67] G. Nooren,[53] J. C. C. Noris,[2] J. Norman,[128] A. Nyanin,[83] J. Nystrand,[21] H. Oeschler,[96] S. Oh,[143] A. Ohlson,[96,34] T. Okubo,[46] L. Olah,[142] J. Oleniacz,[140] A. C. Oliveira Da Silva,[123] M. H. Oliver,[143] J. Onderwaater,[100] C. Oppedisano,[113] R. Orava,[45] M. Oravec,[118] A. Ortiz Velasquez,[62] A. Oskarsson,[33] J. Otwinowski,[120] K. Oyama,[77] M. Ozdemir,[60] Y. Pachmayer,[96] V. Pacik,[84] D. Pagano,[137] P. Pagano,[29] G. Paić,[62] S. K. Pal,[139] P. Palni,[7] J. Pan,[141] A. K. Pandey,[47] S. Panebianco,[65] V. Papikyan,[1] G. S. Pappalardo,[109] P. Pareek,[48] J. Park,[50] W. J. Park,[100] S. Parmar,[91] A. Passfeld,[61] V. Paticchio,[106] R. N. Patra,[139] B. Paul,[113] H. Pei,[7] T. Peitzmann,[53] X. Peng,[7] L. G. Pereira,[63] H. Pereira Da Costa,[65] D. Peresunko,[83,76] E. Perez Lezama,[60] V. Peskov,[60] Y. Pestov,[5] V. Petráček,[38] V. Petrov,[114] M. Petrovici,[80] C. Petta,[27] R. P. Pezzi,[63] S. Piano,[112] M. Pikna,[37] P. Pillot,[116] L. O. D. L. Pimentel,[84] O. Pinazza,[107,34] L. Pinsky,[126] D. B. Piyarathna,[126] M. Płoskoń,[75] M. Planinic,[133] J. Pluta,[140] S. Pochybova,[142] P. L. M. Podesta-Lerma,[122] M. G. Poghosyan,[88] B. Polichtchouk,[114] N. Poljak,[133] W. Poonsawat,[117] A. Pop,[80] H. Poppenborg,[61] S. Porteboeuf-Houssais,[71] J. Porter,[75] J. Pospisil,[87] V. Pozdniakov,[67] S. K. Prasad,[4] R. Preghenella,[34,107] F. Prino,[113] C. A. Pruneau,[141] I. Pshenichnov,[52] M. Puccio,[25] G. Puddu,[23] P. Pujahari,[141] V. Punin,[102] J. Putschke,[141] H. Qvigstad,[20] A. Rachevski,[112] S. Raha,[4] S. Rajput,[93] J. Rak,[127] A. Rakotozafindrabe,[65] L. Ramello,[31] F. Rami,[135] D. B. Rana,[126] R. Raniwala,[94] S. Raniwala,[94] S. S. Räsänen,[45] B. T. Rascanu,[60] D. Rathee,[91] V. Ratza,[44] I. Ravasenga,[30] K. F. Read,[88,129] K. Redlich,[79] A. Rehman,[21] P. Reichelt,[60] F. Reidt,[34] X. Ren,[7] R. Renfordt,[60] A. R. Reolon,[73] A. Reshetin,[52] K. Reygers,[96] V. Riabov,[89] R. A. Ricci,[74] T. Richert,[53,33] M. Richter,[20] P. Riedler,[34] W. Riegler,[34] F. Riggi,[27] C. Ristea,[58] M. Rodríguez Cahuantzi,[2] K. Røed,[20] E. Rogochaya,[67] D. Rohr,[41] D. Röhrich,[21] P. S. Rokita,[140] F. Ronchetti,[34,73] L. Ronflette,[116] P. Rosnet,[71] A. Rossi,[28] A. Rotondi,[136] F. Roukoutakis,[78] A. Roy,[48] C. Roy,[135] P. Roy,[103] A. J. Rubio Montero,[10] R. Rui,[24] R. Russo,[25] A. Rustamov,[82] E. Ryabinkin,[83] Y. Ryabov,[89] A. Rybicki,[120] S. Saarinen,[45] S. Sadhu,[139] S. Sadovsky,[114] K. Šafařík,[34] S. K. Saha,[139] B. Sahlmuller,[60] B. Sahoo,[47] P. Sahoo,[48]

R. Sahoo,[48] S. Sahoo,[57] P. K. Sahu,[57] J. Saini,[139] S. Sakai,[73,132] M. A. Saleh,[141] J. Salzwedel,[18] S. Sambyal,[93] V. Samsonov,[76,89] A. Sandoval,[64] D. Sarkar,[139] N. Sarkar,[139] P. Sarma,[43] M. H. P. Sas,[53] E. Scapparone,[107] F. Scarlassara,[28] R. P. Scharenberg,[98] H. S. Scheid,[60] C. Schiaua,[80] R. Schicker,[96] C. Schmidt,[100] H. R. Schmidt,[95] M. O. Schmidt,[96] M. Schmidt,[95] J. Schukraft,[34] Y. Schutz,[116,135,34] K. Schwarz,[100] K. Schweda,[100] G. Scioli,[26] E. Scomparin,[113] R. Scott,[129] M. Šefčík,[39] J. E. Seger,[90] Y. Sekiguchi,[131] D. Sekihata,[46] I. Selyuzhenkov,[100] K. Senosi,[66] S. Senyukov,[3,135,34] E. Serradilla,[64,10] P. Sett,[47] A. Sevcenco,[58] A. Shabanov,[52] A. Shabetai,[116] O. Shadura,[3] R. Shahoyan,[34] A. Shangaraev,[114] A. Sharma,[93] A. Sharma,[91] M. Sharma,[93] M. Sharma,[93] N. Sharma,[129,91] A. I. Sheikh,[139] K. Shigaki,[46] Q. Shou,[7] K. Shtejer,[25,9] Y. Sibiriak,[83] S. Siddhanta,[108] K. M. Sielewicz,[34] T. Siemiarczuk,[79] D. Silvermyr,[33] C. Silvestre,[72] G. Simatovic,[133] G. Simonetti,[34] R. Singaraju,[139] R. Singh,[81] S. Singha,[81] V. Singhal,[139] T. Sinha,[103] B. Sitar,[37] M. Sitta,[31] T. B. Skaali,[20] M. Slupecki,[127] N. Smirnov,[143] R. J. M. Snellings,[53] T. W. Snellman,[127] J. Song,[99] M. Song,[144] F. Soramel,[28] S. Sorensen,[129] F. Sozzi,[100] E. Spiriti,[73] I. Sputowska,[120] B. K. Srivastava,[98] J. Stachel,[96] I. Stan,[58] P. Stankus,[88] E. Stenlund,[33] J. H. Stiller,[96] D. Stocco,[116] P. Strmen,[37] A. A. P. Suaide,[123] T. Sugitate,[46] C. Suire,[51] M. Suleymanov,[15] M. Suljic,[24] R. Sultanov,[54] M. Šumbera,[87] S. Sumowidagdo,[49] K. Suzuki,[115] S. Swain,[57] A. Szabo,[37] I. Szarka,[37] A. Szczepankiewicz,[140] M. Szymanski,[140] U. Tabassam,[15] J. Takahashi,[124] G. J. Tambave,[21] N. Tanaka,[132] M. Tarhini,[51] M. Tariq,[17] M. G. Tarzila,[80] A. Tauro,[34] G. Tejeda Muñoz,[2] A. Telesca,[34] K. Terasaki,[131] C. Terrevoli,[28] B. Teyssier,[134] D. Thakur,[48] S. Thakur,[139] D. Thomas,[121] R. Tieulent,[134] A. Tikhonov,[52] A. R. Timmins,[126] A. Toia,[60] S. Tripathy,[48] S. Trogolo,[25] G. Trombetta,[32] V. Trubnikov,[3] W. H. Trzaska,[127] B. A. Trzeciak,[53] T. Tsuji,[131] A. Tumkin,[102] R. Turrisi,[110] T. S. Tveter,[20] K. Ullaland,[21] E. N. Umaka,[126] A. Uras,[134] G. L. Usai,[23] A. Utrobicic,[133] M. Vala,[118,55] J. Van Der Maarel,[53] J. W. Van Hoorne,[34] M. van Leeuwen,[53] T. Vanat,[87] P. Vande Vyvre,[34] D. Varga,[142] A. Vargas,[2] M. Vargyas,[127] R. Varma,[47] M. Vasileiou,[78] A. Vasiliev,[83] A. Vauthier,[72] O. Vázquez Doce,[97,35] V. Vechernin,[138] A. M. Veen,[53] A. Velure,[21] E. Vercellin,[25] S. Vergara Limón,[2] R. Vernet,[8] R. Vértesi,[142] L. Vickovic,[119] S. Vigolo,[53] J. Viinikainen,[127] Z. Vilakazi,[130] O. Villalobos Baillie,[104] A. Villatoro Tello,[2] A. Vinogradov,[83] L. Vinogradov,[138] T. Virgili,[29] V. Vislavicius,[33] A. Vodopyanov,[67] M. A. Völkl,[96] K. Voloshin,[54] S. A. Voloshin,[141] G. Volpe,[32] B. von Haller,[34] I. Vorobyev,[97,35] D. Voscek,[118] D. Vranic,[34,100] J. Vrláková,[39] B. Wagner,[21] J. Wagner,[100] H. Wang,[53] M. Wang,[7] D. Watanabe,[132] Y. Watanabe,[131] M. Weber,[115] S. G. Weber,[100] D. F. Weiser,[96] J. P. Wessels,[61] U. Westerhoff,[61] A. M. Whitehead,[92] J. Wiechula,[60] J. Wikne,[20] G. Wilk,[79] J. Wilkinson,[96] G. A. Willems,[61] M. C. S. Williams,[107] B. Windelband,[96] W. E. Witt,[129] S. Yalcin,[70] P. Yang,[7] S. Yano,[46] Z. Yin,[7] H. Yokoyama,[132,72] I.-K. Yoo,[34,99] J. H. Yoon,[50] V. Yurchenko,[3] V. Zaccolo,[84,113] A. Zaman,[15] C. Zampolli,[34] H. J. C. Zanoli,[123] S. Zaporozhets,[67] N. Zardoshti,[104] A. Zarochentsev,[138] P. Závada,[56] N. Zaviyalov,[102] H. Zbroszczyk,[140] M. Zhalov,[89] H. Zhang,[21,7] X. Zhang,[7,75] Y. Zhang,[7] C. Zhang,[53] Z. Zhang,[7] C. Zhao,[20] N. Zhigareva,[54] D. Zhou,[7] Y. Zhou,[84] Z. Zhou,[21] H. Zhu,[21,7] J. Zhu,[7,116] X. Zhu,[7] A. Zichichi,[12,26] A. Zimmermann,[96] M. B. Zimmermann,[34,61] S. Zimmermann,[115] G. Zinovjev,[3] and J. Zmeskal[115]

(ALICE Collaboration)

[1]*A. I. Alikhanyan National Science Laboratory (Yerevan Physics Institute) Foundation, Yerevan, Armenia*
[2]*Benemérita Universidad Autónoma de Puebla, Puebla, Mexico*
[3]*Bogolyubov Institute for Theoretical Physics, Kiev, Ukraine*
[4]*Bose Institute, Department of Physics and Centre for Astroparticle Physics and Space Science (CAPSS), Kolkata, India*
[5]*Budker Institute for Nuclear Physics, Novosibirsk, Russia*
[6]*California Polytechnic State University, San Luis Obispo, California, USA*
[7]*Central China Normal University, Wuhan, China*
[8]*Centre de Calcul de l'IN2P3, Villeurbanne, Lyon, France*
[9]*Centro de Aplicaciones Tecnológicas y Desarrollo Nuclear (CEADEN), Havana, Cuba*
[10]*Centro de Investigaciones Energéticas Medioambientales y Tecnológicas (CIEMAT), Madrid, Spain*
[11]*Centro de Investigación y de Estudios Avanzados (CINVESTAV), Mexico City and Mérida, Mexico*
[12]*Centro Fermi - Museo Storico della Fisica e Centro Studi e Ricerche "Enrico Fermi", Rome, Italy*
[13]*Chicago State University, Chicago, Illinois, USA*
[14]*China Institute of Atomic Energy, Beijing, China*
[15]*COMSATS Institute of Information Technology (CIIT), Islamabad, Pakistan*
[16]*Departamento de Física de Partículas and IGFAE, Universidad de Santiago de Compostela, Santiago de Compostela, Spain*
[17]*Department of Physics, Aligarh Muslim University, Aligarh, India*
[18]*Department of Physics, Ohio State University, Columbus, Ohio, USA*
[19]*Department of Physics, Sejong University, Seoul, South Korea*
[20]*Department of Physics, University of Oslo, Oslo, Norway*
[21]*Department of Physics and Technology, University of Bergen, Bergen, Norway*
[22]*Dipartimento di Fisica dell'Università "La Sapienza" and Sezione INFN, Rome, Italy*
[23]*Dipartimento di Fisica dell'Università and Sezione INFN, Cagliari, Italy*
[24]*Dipartimento di Fisica dell'Università and Sezione INFN, Trieste, Italy*
[25]*Dipartimento di Fisica dell'Università and Sezione INFN, Turin, Italy*

[26]*Dipartimento di Fisica e Astronomia dell'Università and Sezione INFN, Bologna, Italy*
[27]*Dipartimento di Fisica e Astronomia dell'Università and Sezione INFN, Catania, Italy*
[28]*Dipartimento di Fisica e Astronomia dell'Università and Sezione INFN, Padova, Italy*
[29]*Dipartimento di Fisica "E. R. Caianiello" dell'Università and Gruppo Collegato INFN, Salerno, Italy*
[30]*Dipartimento DISAT del Politecnico and Sezione INFN, Turin, Italy*
[31]*Dipartimento di Scienze e Innovazione Tecnologica dell'Università del Piemonte Orientale and INFN Sezione di Torino, Alessandria, Italy*
[32]*Dipartimento Interateneo di Fisica "M. Merlin" and Sezione INFN, Bari, Italy*
[33]*Division of Experimental High Energy Physics, University of Lund, Lund, Sweden*
[34]*European Organization for Nuclear Research (CERN), Geneva, Switzerland*
[35]*Excellence Cluster Universe, Technische Universität München, Munich, Germany*
[36]*Faculty of Engineering, Bergen University College, Bergen, Norway*
[37]*Faculty of Mathematics, Physics and Informatics, Comenius University, Bratislava, Slovakia*
[38]*Faculty of Nuclear Sciences and Physical Engineering, Czech Technical University in Prague, Prague, Czech Republic*
[39]*Faculty of Science, P. J. Šafárik University, Košice, Slovakia*
[40]*Faculty of Technology, Buskerud and Vestfold University College, Tonsberg, Norway*
[41]*Frankfurt Institute for Advanced Studies, Johann Wolfgang Goethe-Universität Frankfurt, Frankfurt, Germany*
[42]*Gangneung-Wonju National University, Gangneung, South Korea*
[43]*Gauhati University, Department of Physics, Guwahati, India*
[44]*Helmholtz-Institut für Strahlen- und Kernphysik, Rheinische Friedrich-Wilhelms-Universität Bonn, Bonn, Germany*
[45]*Helsinki Institute of Physics (HIP), Helsinki, Finland*
[46]*Hiroshima University, Hiroshima, Japan*
[47]*Indian Institute of Technology Bombay (IIT), Mumbai, India*
[48]*Indian Institute of Technology Indore, Indore, India*
[49]*Indonesian Institute of Sciences, Jakarta, Indonesia*
[50]*Inha University, Incheon, South Korea*
[51]*Institut de Physique Nucléaire d'Orsay (IPNO), Université Paris-Sud, CNRS-IN2P3, Orsay, France*
[52]*Institute for Nuclear Research, Academy of Sciences, Moscow, Russia*
[53]*Institute for Subatomic Physics of Utrecht University, Utrecht, Netherlands*
[54]*Institute for Theoretical and Experimental Physics, Moscow, Russia*
[55]*Institute of Experimental Physics, Slovak Academy of Sciences, Košice, Slovakia*
[56]*Institute of Physics, Academy of Sciences of the Czech Republic, Prague, Czech Republic*
[57]*Institute of Physics, Bhubaneswar, India*
[58]*Institute of Space Science (ISS), Bucharest, Romania*
[59]*Institut für Informatik, Johann Wolfgang Goethe-Universität Frankfurt, Frankfurt, Germany*
[60]*Institut für Kernphysik, Johann Wolfgang Goethe-Universität Frankfurt, Frankfurt, Germany*
[61]*Institut für Kernphysik, Westfälische Wilhelms-Universität Münster, Münster, Germany*
[62]*Instituto de Ciencias Nucleares, Universidad Nacional Autónoma de México, Mexico City, Mexico*
[63]*Instituto de Física, Universidade Federal do Rio Grande do Sul (UFRGS), Porto Alegre, Brazil*
[64]*Instituto de Física, Universidad Nacional Autónoma de México, Mexico City, Mexico*
[65]*IRFU, CEA, Université Paris-Saclay, F-91191 Gif-sur-Yvette, France, Saclay, France*
[66]*iThemba LABS, National Research Foundation, Somerset West, South Africa*
[67]*Joint Institute for Nuclear Research (JINR), Dubna, Russia*
[68]*Konkuk University, Seoul, South Korea*
[69]*Korea Institute of Science and Technology Information, Daejeon, South Korea*
[70]*KTO Karatay University, Konya, Turkey*
[71]*Laboratoire de Physique Corpusculaire (LPC), Clermont Université, Université Blaise Pascal, CNRS–IN2P3, Clermont-Ferrand, France*
[72]*Laboratoire de Physique Subatomique et de Cosmologie, Université Grenoble-Alpes, CNRS-IN2P3, Grenoble, France*
[73]*Laboratori Nazionali di Frascati, INFN, Frascati, Italy*
[74]*Laboratori Nazionali di Legnaro, INFN, Legnaro, Italy*
[75]*Lawrence Berkeley National Laboratory, Berkeley, California, USA*
[76]*Moscow Engineering Physics Institute, Moscow, Russia*
[77]*Nagasaki Institute of Applied Science, Nagasaki, Japan*
[78]*National and Kapodistrian University of Athens, Physics Department, Athens, Greece, Athens, Greece*
[79]*National Centre for Nuclear Studies, Warsaw, Poland*
[80]*National Institute for Physics and Nuclear Engineering, Bucharest, Romania*
[81]*National Institute of Science Education and Research, Bhubaneswar, India*
[82]*National Nuclear Research Center, Baku, Azerbaijan*
[83]*National Research Centre Kurchatov Institute, Moscow, Russia*
[84]*Niels Bohr Institute, University of Copenhagen, Copenhagen, Denmark*

[85]*Nikhef, Nationaal instituut voor subatomaire fysica, Amsterdam, Netherlands*
[86]*Nuclear Physics Group, STFC Daresbury Laboratory, Daresbury, United Kingdom*
[87]*Nuclear Physics Institute, Academy of Sciences of the Czech Republic, Řež u Prahy, Czech Republic*
[88]*Oak Ridge National Laboratory, Oak Ridge, Tennessee, USA*
[89]*Petersburg Nuclear Physics Institute, Gatchina, Russia*
[90]*Physics Department, Creighton University, Omaha, Nebraska, USA*
[91]*Physics Department, Panjab University, Chandigarh, India*
[92]*Physics Department, University of Cape Town, Cape Town, South Africa*
[93]*Physics Department, University of Jammu, Jammu, India*
[94]*Physics Department, University of Rajasthan, Jaipur, India*
[95]*Physikalisches Institut, Eberhard Karls Universität Tübingen, Tübingen, Germany*
[96]*Physikalisches Institut, Ruprecht-Karls-Universität Heidelberg, Heidelberg, Germany*
[97]*Physik Department, Technische Universität München, Munich, Germany*
[98]*Purdue University, West Lafayette, Indiana, USA*
[99]*Pusan National University, Pusan, South Korea*
[100]*Research Division and ExtreMe Matter Institute EMMI, GSI Helmholtzzentrum für Schwerionenforschung GmbH, Darmstadt, Germany*
[101]*Rudjer Bošković Institute, Zagreb, Croatia*
[102]*Russian Federal Nuclear Center (VNIIEF), Sarov, Russia*
[103]*Saha Institute of Nuclear Physics, Kolkata, India*
[104]*School of Physics and Astronomy, University of Birmingham, Birmingham, United Kingdom*
[105]*Sección Física, Departamento de Ciencias, Pontificia Universidad Católica del Perú, Lima, Peru*
[106]*Sezione INFN, Bari, Italy*
[107]*Sezione INFN, Bologna, Italy*
[108]*Sezione INFN, Cagliari, Italy*
[109]*Sezione INFN, Catania, Italy*
[110]*Sezione INFN, Padova, Italy*
[111]*Sezione INFN, Rome, Italy*
[112]*Sezione INFN, Trieste, Italy*
[113]*Sezione INFN, Turin, Italy*
[114]*SSC IHEP of NRC Kurchatov institute, Protvino, Russia*
[115]*Stefan Meyer Institut für Subatomare Physik (SMI), Vienna, Austria*
[116]*SUBATECH, Ecole des Mines de Nantes, Université de Nantes, CNRS-IN2P3, Nantes, France*
[117]*Suranaree University of Technology, Nakhon Ratchasima, Thailand*
[118]*Technical University of Košice, Košice, Slovakia*
[119]*Technical University of Split FESB, Split, Croatia*
[120]*The Henryk Niewodniczanski Institute of Nuclear Physics, Polish Academy of Sciences, Cracow, Poland*
[121]*The University of Texas at Austin, Physics Department, Austin, Texas, USA*
[122]*Universidad Autónoma de Sinaloa, Culiacán, Mexico*
[123]*Universidade de São Paulo (USP), São Paulo, Brazil*
[124]*Universidade Estadual de Campinas (UNICAMP), Campinas, Brazil*
[125]*Universidade Federal do ABC, Santo Andre, Brazil*
[126]*University of Houston, Houston, Texas, USA*
[127]*University of Jyväskylä, Jyväskylä, Finland*
[128]*University of Liverpool, Liverpool, United Kingdom*
[129]*University of Tennessee, Knoxville, Tennessee, USA*
[130]*University of the Witwatersrand, Johannesburg, South Africa*
[131]*University of Tokyo, Tokyo, Japan*
[132]*University of Tsukuba, Tsukuba, Japan*
[133]*University of Zagreb, Zagreb, Croatia*
[134]*Université de Lyon, Université Lyon 1, CNRS/IN2P3, IPN-Lyon, Villeurbanne, Lyon, France*
[135]*Université de Strasbourg, CNRS, IPHC UMR 7178, F-67000 Strasbourg, France, Strasbourg, France*
[136]*Università degli Studi di Pavia, Pavia, Italy*
[137]*Università di Brescia, Brescia, Italy*
[138]*V. Fock Institute for Physics, St. Petersburg State University, St. Petersburg, Russia*
[139]*Variable Energy Cyclotron Centre, Kolkata, India*
[140]*Warsaw University of Technology, Warsaw, Poland*
[141]*Wayne State University, Detroit, Michigan, USA*
[142]*Wigner Research Centre for Physics, Hungarian Academy of Sciences, Budapest, Hungary*
[143]*Yale University, New Haven, Connecticut, USA*

[144] *Yonsei University, Seoul, South Korea*
[145] *Zentrum für Technologietransfer und Telekommunikation (ZTT), Fachhochschule Worms, Worms, Germany*

[*] Deceased.
[†] Also at Georgia State University, Atlanta, Georgia, USA.
[‡] Also at Also at Department of Applied Physics, Aligarh Muslim University, Aligarh, India.
[§] Also at M. V. Lomonosov Moscow State University, D. V. Skobeltsyn Institute of Nuclear, Physics, Moscow, Russia.